Sensing Direction of Human Motion Using Single-Input-Single-Output (SISO) Channel Model and Neural Networks

SAMEER AHMAD BHAT[1,2], **MUNEER AHMAD DAR**[2], **PIOTR SZCZUKO**[1], **DALIA ALYAHYA**[3], **AND FARHANA MUSTAFA**[4]

[1]Department of Multimedia Systems, Gdańsk University of Technology, 80-233 Gdańsk, Poland
[2]Department of Computer Science, National Institute of Electronics and Information Technology, Jammu and Kashmir 191132, India
[3]Department of Instructional Technology, King Saud University, Riyadh 11362, Saudi Arabia
[4]Department of Electronics and Instrumentation Technology, University of Kashmir, Jammu and Kashmir 190006, India

Corresponding author: Sameer Ahmad Bhat (sameer.bhat@pg.edu.pl)

ABSTRACT Object detection Through-the-Walls enables localization and identification of hidden objects behind the walls. While numerous studies have exploited Channel State Information of Multiple Input Multiple Output (MIMO) WiFi and radar devices in association with Artificial Intelligence based algorithms (AI) to detect and localize objects behind walls, this study proposes a novel non-invasive Through-the-Walls human motion direction prediction system based on a Single-Input-Single-Output (SISO) communication channel model and Shallow Neural Network (SNN). The motion direction prediction accuracy of SNN is highlighted against the other types of Machine Learning (ML) models. The comparative analysis of models in this study shows that unique human movement patterns, superimposed on received pilot radio signal, can be classified precisely by SNN, with an accuracy of approximately 89.13% compared to the other ML based models. The results of this study would guide scholars, active in developing human motion recognition systems, intrusion detection systems, or Well-being and healthcare systems, and in processes that innovate and improve processing techniques for monitoring and control.

INDEX TERMS Artificial intelligence, artificial neural networks, classification algorithms, data analysis, feature extraction, feedforward neural networks, machine learning, modeling, neural networks, pattern analysis, software radio.

NOMENCLATURE

CFR	Channel Frequency Response.
CNN	Convolutional Neural Networks.
COTS	Commercially available Off-the-self.
CSI	Channel State Information.
CW	Continuous Wave.
DNN	Deep Neural Networks.
DTW	Dynamic Time Wrapping.
DWT	Discrete Wavelet Transform.
FCNN	Fully Connected Neural Network.
FPGA	Field Programmable Gate Arrays.
HAR	Human Activity Recognition.
HCI	Human-Computer interaction.
HMM	Hidden Markov Model.
HMR	Human Motion Recognition.
ISM	Industrial, Scientific and Medical band.
KNN	K-Nearest Neighbours.
LDA	Linear Discriminant Analysis.
LOS	Line of Sight.
MAF	Moving Average Filter.
MEMS	Micro-electromechanical systems.
MIMO	Multiple Input Multiple Output.
MLP	Multi-layer Perception.
mmWave	Millimeter Wave.
NLOS	Non Light of Sight.
NNN	Narrow Neural Networks.
ODTTW	Object Detection Through-The-Walls.
PCA	Principal Component Analysis.
PSD	Power Spectral Density.
RCT	Randomized Control Trial.
RFPSP	Radio Frequency Pilot Signal Processor.
RSK	Real-Signal Kurtosis.
RSS	Received Signal Strength.

The associate editor coordinating the review of this manuscript and approving it for publication was Hiram Ponce.

RSSI	Received Radio Signal Strength Indicator.
RX	USRP based Receiver.
SDR	Software Defined Radio.
SISO	Single Input Single Output.
SNN	Shallow Neural Network.
SVM	Support Vector Machines.
TPR	True Positive Rate.
TWRI	Through Wall Radar Imaging.
TX	USRP based Transmitter.
USRP	Universal Software Radio Peripheral.
UWB	Ultra-wideband.

I. INTRODUCTION

Recent advancements in wireless and communication technology are driving researchers towards developing systems that exploit Channel State Information (CSI) of radio communication devices for localization and pattern recognition based applications. Several research studies focussed on areas of human motion detection, gesture detection, and facial recognition systems have been proposed [1]–[5]. Wireless communication devices available in the markets at present are grounded on Software Defined Radio (SDR) sub-units that enable support to multi radio subcarrier transmission, thereby enabling communication of different types of data. These SDR sub-units facilitate the acquisition of CSI in wireless communication devices, and the collected CSI data is then explored to uncover hidden human motion patterns. Some Commercially Available Off-The-Shelf (COTS) devices even output CSI directly via their in-built radio subsystems [6]. Likewise, WiFi devices available today, also output CSI and outperform against the other human motion sensing systems. However, Human Activity Recognition (HAR) processes using WiFi based solutions prerequisite acquisition of CSI for accurate estimation and prediction of human activities [7], [8].

A review of recent studies unveils that CSI signals show randomized behavioral patterns. This randomized behavior prevails due to signal reflections in the multipath signal propagation and mainly serves as a source of distortion in the received signals [9]–[11]. The statistical random variations observed in the CSI data primarily exist due to the Non Line of sight (NLOS) propagation characteristics. Any errors introduced by the reflections, scattering, and diffractions of signals are mainly considered as obstacles in signal propagation [12]. Random patterns in CSI exist due to the dynamic motion of objects in the near vicinity of the transmission source that inevitably influence the elementary behaviour of received signals. Although CSI employs physical layer properties to differentiate between the amplitude and phase characteristics whilst being sensitive to the dynamics of the environment, the multipath effect is observed to be constructive, when it comes to its applications in localization systems that are based on fingerprinting [13]. While the amplitude of CSI could be a stable metric, the added external noise to the signal from the system and the environment distorts the signal considerably [14]. The distance between a transmitter and receiver, and radio reflection, refraction, diffraction, absorption, polarization, and scattering, termed as multipath effects, considerably attenuate the amplitude and introduce phase shift in CSI signals [15]. Apparently, the complex nature of acquired CSI data revealing random probability distribution, requires efficient processing mechanisms of noise removal and signal decomposition, before some meaningful information can be extracted from it, or in particular signal features that are imperative in the pattern recognition processes and applications. To identify the behavioral characteristics or patterns in any given CSI dataset, successive remarkable attempts have been made so far by the research communities, uncovering the potential of CSI for human motion recognition. Various approaches of signal processing have been used so far, for instance, Discrete Wavelet Transform (DWT) is used for noise removal and Linear Discriminant Analysis (LDA) for feature engineering by [16], feature extraction using Principal Component Analysis (PCA) by [9], [10], [17], the CLEAN algorithm by [18], Doppler spectrum by [19] and even scale and time shift projections by [16]. Signal processing methods as such prerequisite high speed processing elements, and in addition to being process intensive, running these algorithms on tiny or resource constrained hardware devices may not be an optimal solution. Also, the primitives - rising edges, falling edges, and pauses defined at the primitive layer in [16] attempt to address issues as mentioned, however, in a generic sense. Therefore, the need to reduce the complexity of CSI processing and application of innovative filtering techniques merely result in an increase in the number of processing elements as well as leads to additional system costs.

Whereas numerous research studies based on WiFi have been used for developing applications for localization and pattern recognition, the resulting systems are highly accurate in recognizing human activities, in particular human motion, and mostly employ either machine learning or deep learning algorithms for pattern recognition or classification. CSI can reveal patterns in the data, which come from different domains, for instance, motion sensing systems, object recognition systems, and pose estimation. However, it requires processing, modelling, and training specific to the each domain. WiFi sensing performance relies mostly on noises and outliers that exist in the collected raw CSI data [9], and the CSI data acquisition with off-the-shelf WiFi cards, may not always be a readily available option, since CSI data acquisition features are unavailable in some WiFI cards. In addition, there are concerns relating to processing complexity of CSI signals, portability of WiFi devices, adaptability to current networks, unreliability to due fading channel propagation, lower precision due to random nature of CSI, and inefficient system designs due to complex signal processing architectures. The radio subunits provide CSI that often requires hardware and software signal processing mechanisms, and subsequently the developed systems adumbrate need of complex signal processing circuitry.

Although the motion detection accuracy of Wifi is high compared to the other radio devices, CSI data is dependent on the availability of multiple WiFi channels for consistent monitoring of activities under consideration. If one of the channel experiences interruption, the detected activity, for example human motion prediction, accuracy may decrease significantly. This leads us to propose a single communication channel only for activity recognition purposes instead of employing multiple radio communication channels. The proposed method alleviates the level of processing, when compared to the processing used for multiple CSI sub-carriers, and implements a Single Input Single Output (SISO) channel model for activity recognition, in this study human motion direction prediction. Using SISO, there exists a single transceiver pair, modelling the system to enable detection of human motion. This study presents a testbed for modelling SISO communication system model, and an experimental setup to evaluate the prediction accuracy of the single channel based human motion direction prediction system. A human surveillance system is presented that predicts the direction of human motion under the realm of detection through the walls. For human motion classification, this study employs machine learning models to identify different human motion patterns of four different humans employed in this study. The motion patterns were collected in a controlled lab environment. Therefore, the study extends scope of the current research in human activity or motion recognition systems, and proposes the development of an efficient human motion direction identification system. In addition to demonstrating the SISO model based human motion direction prediction, the study also highlights the practical implementation of SDRs for human motion surveillance and activity monitoring.

In this paper, a Shallow Neural network [20] based system model is proposed that acquires and processes received Radio Signal Strength (RSS) data from a SISO communication channel to identify the direction of human motion, through the walls. A testbed is setup and configured in a real time scenario to validate the proposed model, and estimate the detection accuracy of the proposed system model. The proposed system processes unique human motion signatures, superimposed on the RSS, and then attempts to unveil the direction of human motion from RSS using various machine learning models. In abreast to showcasing predictions on **human motion direction**, which CSI-based and other HAR studies have never focused before, the study shows direction prediction accuracies resulted by different machine learning models for comparative analysis, enabling us to determine the best prediction model. The study hypothesis bases on the assumption that Shallow Neural Networks (SNNs) can provide the optimal human motion direction prediction accuracy (SNNs) by classifying the human motion patterns, acquired from a continuous time pilot carrier signal transmission. Therefore, SNN prediction model is implemented in LabVIEW to validate the prediction accuracy of the devised human motion direction recognition model, in addition to training various other machine learning models for comparison. The study

results show that SNNs show higher prediction accuracies than other machine learning models, whilst presenting a light network model compared to the deep learning frameworks with multiple hidden layers, typically implemented in human motion recognition systems using WiFi.

A. CONTRIBUTION
This study proposes a system model for human motion detection through the walls, and employs just a single carrier frequency of 2.4GHz, enabling detection human motion and to trace the direction of human motion using a SISO based channel model. The main contributions of this study are listed here under:

- The study proposes a testbed to validate the proof-of-concept i.e., to identify the **direction of human motion** in indoor environments using SNN. The proposed testbed implements a Single Input Single Output (SISO) topology.
- The study provides a system model that enables human motion direction recognition using a single communication channel. SNN is used to predict the six different directional motion patterns of four participants.
- The study provides a novel method to identify the direction of human motion based on Software Defined Radios (SDRs). A case study of human motion surveillance is described to highlight the applications of SDRs in Through the walls human motion sensing and detection.
- The study evaluates accuracy of various machine learning models on the collected human motion dataset. A comparative analysis of SNN with other machine learning models is also given to determine the best prediction model.
- The study provides statistical validation of the two proposed models to determine the efficient model for predicting human motion direction.

B. PROBLEM STATEMENT
From the literature review, we conclude that most of the studies have addressed challenges pertaining to human motion recognition. WiFi and radar sensing technology in association with machine learning and Deep Neural Networks (DNNs) have been widely investigated and applied in numerous applications. The systematic literature review reveals that prolific attempts have been made to address challenges pertaining to human motion recognition. However, there is no research study till date that addresses the challenge of detecting the **direction of human motion** from the RSS of a pilot signal, more specifically with Universal Software Radio Peripherals (USRPs) [21] using omni-directional antennas. Using our proposed method, we the authors of this study claim to be the first to address this challenge, and present a novel method that employs a single Continuous Wave (CW) - a pilot radio subcarrier, and the Shallow neural network for predicting the direction of human motion in a controlled environment.

C. STUDY OUTLINE

The study is organized according to the following sections. Section-II provide a detailed literature review of related studies. Section III discusses a theoretical perspective of the study, while the Section-IV provides the experimental design method. Section-V, method of data collection acquisition using SDRs. Section-VI provides the SNN based machine learning solution to motion pattern analysis and classification, whereas Section-VII discusses study results and compares resulting ML models. Finally in the Section-X, conclusions are presented and suggestions are made for future research in Section

II. RELATED WORK

With the current advancements in wireless communication and sensing technologies, their applications to HAR systems are gaining wider acceptance at global level. In recent years, wireless technologies have played a vital role in the development of HAR systems. HAR is intuitively the main driving technology in human-computer interaction and activity analysis, and is nowadays the promising area of research in the field of artificial intelligence. A number of research studies have focused on issues concerning HAR [16]. HAR methods used in the current ongoing research are broadly divided into three main categories – image processing, wearable sensing devices, and wireless radio signal processing.

In computer vision, using image processing techniques on modelled human motion and analyzing effects in real life settings, are currently driving the development of many industrial and commercial applications [17], [22]. For example, real-time Human Motion Recognition (HMR) [18], systems using radar images responsible for distinguishing human motions [19], intelligent surveillance platforms [23] and many others. In addition to the applied image processing techniques, HMR systems base on various types of sensors such as Micro-electromechanical System (MEMS) Sensors [19], motion sensor using U-Net [24], smartphone-based inertial sensors [25], magnetic field sensors [26], Continuous-Wave Radar Sensors [27] and velocity sensor array [28]. Currently, prolific sensor based HMR systems are widely available, however, research has shown that signals acquired from WiFi devices can help in recognizing human motions and positions [29]. Several WiFi based solutions such as WiAct [30], WiRoI [31], WiDrive [32], WiFi Motion Detection [33], WiTT [23] and many others have be already proposed and implemented.

These WiFi based studies devise solutions based on CSI, which the SDR devices acquire by analyzing the multiple radio sub-carriers. However, preprocessing the CSI is a difficult task on hand and poses several critical challenges whilst deriving human activity information from it. Typically, the quantitative measure of CSI phase reveals that the sampling time mismatch leads to random phase shifts in the signals [34]. Consequently, the devices having same hardware and software architectures, including physical properties may show varying results, even if the devices receive the same type of activity data, as input. The lower sampling rate of processing units within the SDRs results in processing delays, eventually limiting their application in real time systems. While CSI subcarriers are influenced by the dynamic nature of a communication channel and intensity level of noise, extracted CSI data are input to the signal processing units for eliminating the unwanted noise, applying signal transforms, and/or extracting actual motion signals. Next, pre-processed CSI data are input to algorithms that employ modelling, learning, or hybrid algorithmic techniques to deliver the output, targeted at different WiFi based sensing applications. This requires cleansing, processing and analysis of each CSI subcarrier, which in turn demand efficient hardware resources. Moreover, the sensing environments may elevate additional processing demands due to dynamic background of the monitoring environments. The background object elimination algorithms, for instance by [34], may eliminate such effects and estimate likelihood criteria to isolate actual targets from the other environmental entities, however the present estimation criteria demand precise estimations of the noisy descriptor variables that mostly rely on ambient parameters [35].

As far as Hardware devices are concerned, WiFi network cards, for instance Intel 5300 network card, are installed and fixed inside notebooks or desktop computers. The fixed orientation limits their application in testbeds, where user defined orientation is desired to acquire CSI statistics. Similarly, Multiple-Input-Multiple-Output (MIMO) systems [17], [18] employ multiple transmitters and receivers, include multiple antennas for reception and transmission [2], [36]. Increase in hardware and advanced software requirements, extends the level of costs of MIMO devices compared to SISO devices that rely on simple hardware, software and antenna types. MIMO systems adumbrate higher resource requirements including hardware complexity when compared to SISO systems. Individual RF units are prerequisite to process radio signals of each antenna, and MIMO topology employs advanced mathematical or signal processing algorithms that necessitate powerful Digital Signal Processors (DSPs) to execute the developed algorithms. Apparently, increase in the requirement of hardware resources leads to increase in the power requirements. Eventually, complex and computationally intensive signal processing algorithms lead to high battery consumption, thereby draining out batteries faster and decreasing life time of batteries used to drive MIMO devices.

The proliferation of hardware elements as such increases infrastructure and deployment costs, and also limits their applicability in the processes leading to the development of low cost solutions that enable HAR. Some studies also affirm that adding additional subcarrier frequencies in the WiFi recognition process does not help in improving the human recognition accuracy. The study by [10] and [17] reports that CSI acquired with WiFi operating at 5GHz of frequency with 114 and 132 subcarriers, shows 94.0% and 94.1% of True Positive Rate (TPR) only in detection accuracies, respectively. This implies that recognition accuracy

or in other words the TPR is independent of the number of CSI subcarriers, and also proves that employing additional radio subcarriers unlikely shows an increase in the level of human motion recognition accuracy. Hence, HAR systems that implement a number of subcarrier frequencies, demonstrate a limit in the level of accuracy of human motion detection with multi subcarrier channel based systems.

On the other hand, HMR systems grounded on radar sensing technology, immensely eliminate the need of deploying numerous sensors, and are mostly preferred over other sensor based systems. HMR systems based on radar sensor systems have been extensively used in various applications, including surveillance [37], [38], activities concerning search [39], [40] and rescue [41], smart environments [42], [43], and in ambient assisted living [44]–[46]. Research studies, for instance motion capturing system [47], contact-less UWB Radar [48], Magnetic Induction [49] exclusively demonstrate the featured capabilities of non-intrusive motion recognition systems. Among many wireless sensing technologies, radar sensing has emerged as an efficient solution that relatively focuses on areas such as commerce, defense, and security. Although widely used in military and defense services, radar sensing systems are also implemented in Human–Computer Interaction (HCI) in medical applications, in automotive fields and smart sensing systems [50]. Radar technology employing frequencies that range from few GHz to hundreds of GHz (mmWave) is used for medium or very close range sensing, and presents an environmentally robust sensing systems. Recent applications of radar include gesture recognition [51], [52], monitoring patients [53], monitoring movement of Ataxia Patients [54], detection and tracking of the human body [55] and various other applications. Amalgamation of radar sensing devices and Machine learning, particularly ones that work in association with Deep Neural Networks (DNNs), have shown promising results in applications, such as counting number people in a room [56], human identification [57], and even in unknown human classifications [58].

Typical experimentation with radar sensing systems, prerequisite distinguishing factors to be taken into account. The characteristics, such as technology, modulation technique, frequency, communication bandwidth, antenna type, including the processing capability of algorithms, serve as major factors that influence the overall application area of radar based sensing and tracking systems. From our literature review of recent studies, we divide radar sensing technology into four dimensions, *a*) technology *b*) frequency *c*) antenna types *d*) implemented modulation techniques and *e*) Data representation. We consider that these five dimensions are the key factors that affect the overall performance of a human radar based sensing and tracking system, as numerous studies have relied on these parameters so as to achieve higher performance and level of sensing accuracy. The Table-1 lists these five main parameters with corresponding definitions.

Most of the human motion recognition applications implement artificial intelligence based solutions to unveil the hidden characteristics in the data, whereby the data acquired

TABLE 1. Current radar sensing technologies.

Technology	Multiple Input Multiple Output (MIMO) Ultra-Wideband MIMO MIMO Beamforming MIMO + KINET Massive MIMO
Frequencies (GHz)	66-77, 15-17, 10, 4, 3.42, 2.4
Modulation Types	Continuous Wave (CW), Linear Frequency modulation (LFM), Orthogonal Frequency Division Multiplexing (OFDM), Frequency Modulated Continuous Wave (FMCW), Stepped Frequency Continuous Wave (SFCW)
Antenna	Micro-strip, horn, Circular, Dipole, Wall board
Data representation	Imaging (spectrograms, thermal images) Non-imaging (direct transformations)

from radar sensors is typically processed off-line than in actual real time [30]–[34]. Real time human motion recognition applications, in general, exclusively demand lower complexity of signal processing hardware, so as to enable fast and efficient human motion data processing, also require hardware circuitry to ensure active real time response. Nonetheless, to implement the DNN algorithms on a low level hardware architectures is a challenge in itself because DNNs exhibit highly complex architectures that demand high end processing elements employing complex signal processing techniques.

A. RESEARCH MOTIVATION

In recent years, Object Detection Through-The-Walls (ODTTW), has been a major source of attraction to researchers. Due to its wide range of capabilities, ODTTW enables support for security and military defence applications. In a typical ODTTW application, a radar transmitter sends out electromagnetic pulses through the wall to sense the presence of an object, located on the other side of the wall. And the returned signal reflections from a wall and target, are processed to detect the presence of an object. ODTTW does not need to establish any physical contact with objects that lie behind walls, so it allows passive detection of hidden objects. Sensing systems, as such, are categorized as passive sensing systems, exhibit features such as context awareness in close proximity, or monitoring an object that is located on either side of a wall. The method of transmission of radar signals, to detect objects that are located behind walls, finds application in tasks such as surveillance, search and rescue operation, enforcement of law, and other operations that save people's live's [59], [60]. There are other methods as well that help in sensing and localization of objects covered by walls. Sensing methods, as such, employ 60-70 GHz band of spectrum [61]–[64], to passively sense the presence of objects hidden behind the walls. On the other hand, Through Wall Radar Imaging (TWRI) methods are used to reconstruct static targets, as well as to present the information on the
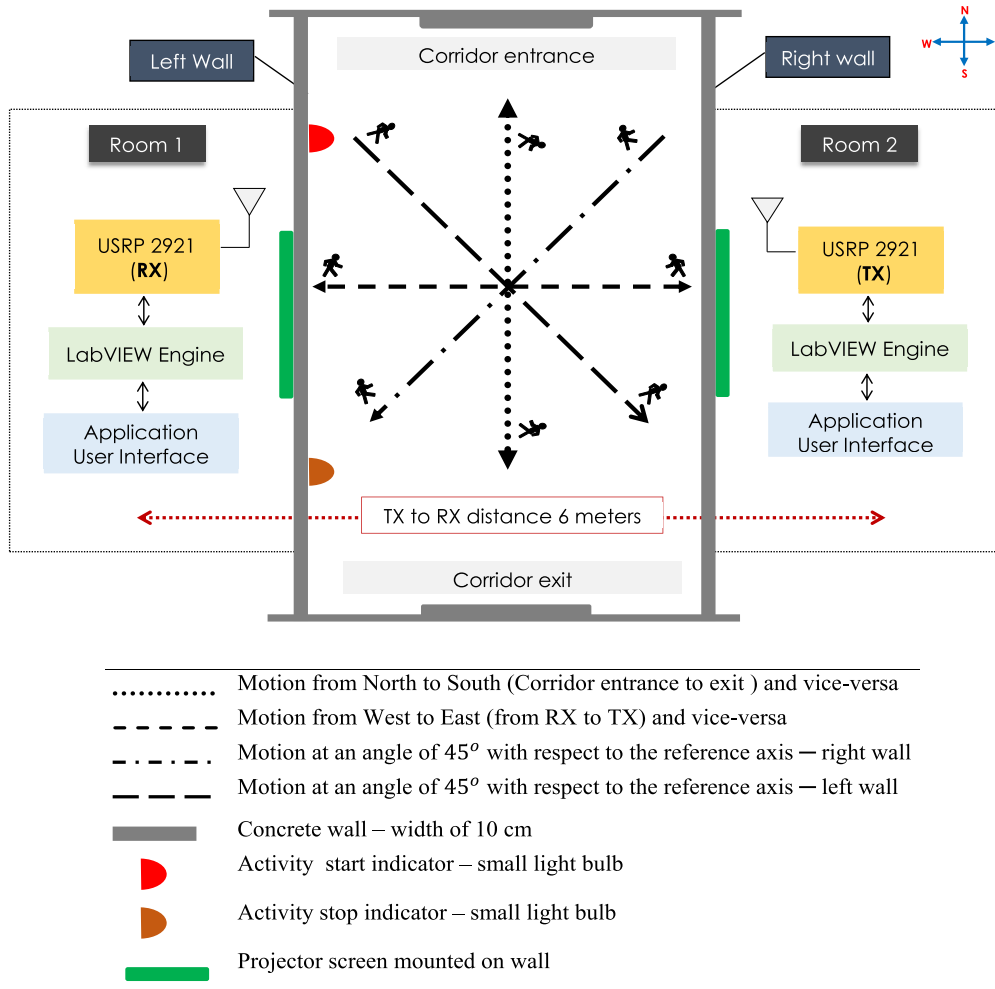
FIGURE 1. Proposed system model human motion direction recognition through walls.

monitored scene of a hidden object. Nevertheless, the parameters defining the characteristics of a wall, and others that define the position there, are necessary, prior conditions to the process rebuilding a scene, although wall parameters are usually unknown in real scenarios [65].

One of the major problems, underlying in environments as such, is the unknown width of a wall or barrier; an essential parameter, which is often neglected in the process of imaging or modelling the background space of a wall. These types of barriers can completely block the transmission of radar signals, if walls are highly dense in their physical structure. However, if the frequencies used for transmission are low, then walls can allow penetration of signals with low frequencies. TWRI studies have mostly focused on stationary objects, but some studies have attempted to model, and investigate scenarios, wherein attempts have been made to localize moving objects [66]. To sense non-moving objects that are covered by walls, two preconditions need to be satisfied. The first condition is to remove clutter from walls, which result in multiple reflections of a radar signal due to the irregular

nature of objects on the wall, and the second is to build an image which models the reconstructed scene of the background [62], [67]. Nonetheless, if the strengths of reflected radar signals, are stronger, due to high density of walls, than the reflected radar signals that emerge, due to a stationary object, lying behind a wall, then the process of detecting an object, becomes very difficult because of clutters that lie in between radar, and a target object [68]. On the other hand, the frequencies that range below the radar frequency band can easily penetrate through walls, and thus enable the detection of objects located behind walls, possibly. Therefore, the frequencies that lie in the range of 2GHz to 5GHz are most suitable for human motion detection.

III. SYSTEM MODEL
Our study design bases on the system model that makes use of SDRs that allow customization at both the hardware and software level. The proposed system model comprises of two SDRs, with one acting as a transmitter and other as receiver. SDRs allow instant software update to be made to the radio

hardware, and this level of customization is achieved through an application programming interface, such as LabVIEW. The LabVIEW application runs on a computer, which sends out control and data commands to the SDR via a USB cable. The software updates made to reconfigure the SDR hardware, make it more easier readjust the system design of SDRs, and SDRs can be programmed, or reprogrammed instantly to meet the local and international commercial guidelines of RF transmission. SDRs are portable devices, allow reconfiguration of hardware parameters such as controlling the IQ rate, bandwidth, data sampling, filtering, and radio internal block circuitry, which include implementation of coding and decoding techniques. The two programmable radio devices are placed 6 meters apart in two lab rooms. SDRs are connected to two desktop computers, with one computer connected to the projector that displays the application interface on the sidewall to indicate to the participant, when to start and stop human walking activity.

To determine the necessary settings of proposed testbed system and their control configurations, this study employed an experimental setup that determines these necessary parameters using the Randomized Control Trial (RCT) method. A topology based on NI-USRPs was designed to collect data of human movements in various directions. The sections next provide the theoretical background of the proposed model, procedure of the experiment design and setup, data collection method, and application of proposed machine learning model to the collected data.

A. BACKGROUND OF SIGNAL PROPAGATION

A transmitted signal propagates from the transmitter to the receiver at a particular frequency of interest. Wireless signals travelling the through space may arrive at the receiver via various paths, and each path typically delays and attenuates the signal. The signal transmission by wireless devices, may encounter many obstacles in communication medium, and the CSI acquired from a radio subsystem provides the Channel Frequency Response (CFR) that describes the propagation behavior of signal through the communication medium. The CFR outsourced by CSI, characterizes the signal transmission from transmitter to the receiver and is expressed by eq(1):

$$H(k; t) = \sum_{q} b_q(t) e^{-j2\pi k \phi_q} \tag{1}$$

where $b_q(t)$ and ϕ_q represents the amplitude attenuation and the propagation delay parameter, respectively. The parameter k represents the frequency of the transmitted carrier or continuous wave. It should be observed that the relocation and movement of the transmitter, receiver, and the ambient entities and humans influence the amplitude $\|H\|$ and phase $\angle H$ of the CSI. This implies that the CSI embeds the effects of objects in the nearby vicinity of the transmitter and receiver, and the observed CSI basically reveals or characterizes the sensed environment, using mathematical modelling. The same rationale governs the implementation of CSI based WiFi sensing systems.

Signal propagation in indoor environments usually follows a similar behaviour showed in the external environments, and the transmitted signal may travel through various path to arrive at the receiver. While the receiver receives the actual transmitted signal, some alias forms arising out of multi path propagation of the actual transmitted signal may also arrive at the receiver [10]. The voltage level (S) of pilot carrier signal available at the receiver is expressed by eq(2):

$$S = \sum_{p=1}^{N} \|S_p\| e^{-j\theta_p} \tag{2}$$

where S_p represents the amplitude of the p_{th} multipath component, θ_p denotes the phase of the p_{th} multipath component and N is the total number of multipath components. S represents the overall signal strength received at the receiver. The Radio Signal Strength (RSS) [10] of pilot measured in terms of decibels scale (dB) is expressed by eq(3):

$$\text{RSSI}_{(\text{dB})} = 10\log_{10}\left(\|S\|^2\right) \tag{3}$$

The level of received signal strength depends on the signal propagation distance, wavelength, and time. Due to dynamics of the environment, the strength of pilot signal varies considerably,in fact even with minor multipath components dynamics. A study by [23] reports that 5 dB of change in the RSSI has been observed over a minute, on an immobile receiver, placed in a controlled lab environment. This implies that the having fixed location for transmitter and receiver is more stable compared to having a mobile setup. Hence, this study makes use of an immobile setup for both the transmitter and receiver, so as to ensure RSSI variations are reduced to minimum possible values.

1) SISO CHANNEL MODEL AND FEATURE EXTRACTION

Using a conventional channel estimation method based on standard-defined pilot sub-carrier arrangement [69], the MIMO channel response is monitored in the frequency domain over k pilot sub-carriers $\lambda \in \mathbb{F} = (\lambda_1, \lambda_2, \cdots, \lambda_k)$. This study develops features based on SISO channel data to identify directional motion patterns. A moving persons' body movements modify the statistical properties of the RSS in the frequency domain, such as the strength moments can evaluate as an average over the time in a given frequency sample. For example, attenuation and fading of RSS due to the body of a person are referenced by the statistical properties, like mean and variance. In the following, the study considers statistics of the overall SISO power frequency profile. The frequency-domain CSI strength vector for link u at time t is defined by eq(27):

$$S_{u,t} = \left[S_{\lambda_1, u, t} \cdots S_{\lambda_k, u, t} \right]^{\mathbb{T}} \tag{4}$$

where CSI $S_{u,t}$ is the strength observed at time $t \in \mathbb{T}$ on sub-carrier $\lambda \in \mathbb{F}$ and link $u \in \mathbb{U}$.

The complex baseband channel response observed on frequency $\lambda \in \mathbb{F}$, over the link $\lambda = \lambda(\beta_t, \beta_r)$ between the

transmitting antenna $\beta_t = (1, \cdots, Z_t)$ and receiving antenna $\beta_r = (1, \cdots, Z_r)$ at time $t \in \mathbb{T}$ is denoted as $H_{\lambda,u,t}$.

Where the index $\lambda \in \mathbb{F} = (\lambda_1, \lambda_2, \cdots, U)$ ranges over the $U = Z_t Z_r$ radio links.

While employing SISO channel model, this study employs and extracts a single channel strength sample only $S_{\lambda_1,1,t}$ from the frequency vector $S_{u,t} = \left[S_{\lambda_1,u,t} \cdots S_{\lambda_k,u,t} \right]^{\mathbb{T}}$.

Where λ_1 represents a single channel pilot radio carrier, and $u = 1$ represents a single communication link.

Six distinctive statistical indicators model the features of corresponding probability function $S_{(\lambda,1,t)} \sim P_{r[S_{f,1,t}]}$, and are defined in the Section–(VI-C).

IV. EXPERIMENTAL SETUP

The experimental method applied to the devised system model (see Fig.1) employs a SISO channel that comprises of one Transmitter (TX) and Receiver (RX) as a pair for the initial testing and setup. The transceiver pair, both have small antennas with omnidirectional radiation pattern and operate in commercial ISM 2.4 GHz band. Antenna specifications are - VERT2450 Dual Band 2.4 to 2.48 GHz and 4.9 to 5.9 GHz omni-directional vertical antenna, at 3dBi Gain. To acquire data, the study sets up six directions for observing six directional human motion patterns and selects four participants for data collection. The environment for the experiment included two adjacent rooms, separated by a common path of a corridor between the two. A desktop computer along with the SDR was setup in each room to devise the proposed testbed for the experiment. The corridor environment was set out to have no obstacles in it's path and provided participants a free space to walk through. The motion patterns of each participant were monitored inside the receiver room, however participants were apprised when to start and stop the motion, i.e. walking, using two indicators mounted on the left wall of the corridor.

A. INSTRUMENT SETUP

Two NI-USRP 2921 [25] SDRs were employed with TX and RX applications, which were developed in LabVIEW [24]. The TX application allowed controlled pilot signal transmission at a frequency of 50KHz, and the RX application was used to estimate the Power Spectral Density (PSD) of pilot signal. TX and RX devices were placed at a distance of 6 meters apart from each other, and the gain of both the devices was set to default i.e. to zero, for the purpose of initial testbed setup.

- **Corridor:** we performed experiments in a corridor environment of our academic building. The corridor dimensions are 2m × 15m, and it has two adjacent rooms in the pathway. In this scenario, there are two NI-USRP devices placed in each one of the rooms, whereby one transmits the 50KHz RF pilot signal and the other device acts as a receiver of transmitted pilot signal. We collected motion fingerprints at six different reference positions in this scenario, while placing the NI-USRPs 6m
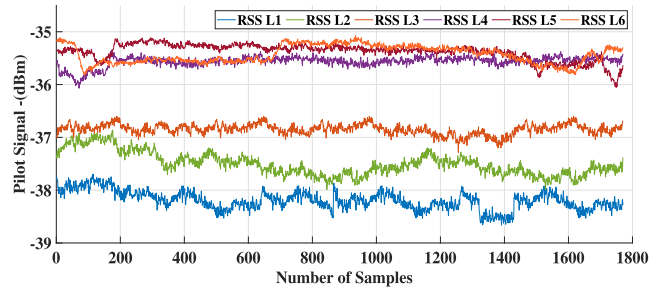

FIGURE 2. The mean variation of 50KHz Pilot signal under no human presence in the corridor. The letter L denotes the six different levels observed signal strengths.

TABLE 2. Optimal gain setting for TX and RX.

TX to RX distance	TX Gain	RX Gain	RSS (dB) (Noise)
6 m	0	0	-99 dB
6 m	50	0	-80 dB
6 m	0	50	-77 dB

apart from the corridor path (see Fig.1). In each reference direction, we collected three datasets consisting of RSS values, for each move of each participant.

- **Initial Testbed Setup and RSS Stabilization:** To test the validity of proposed testbed, first orientation tests were performed to ensure there is minimum level of variation in RSS. Table 2 provides measured values of the power level of RSS on a *dB* scale, while selection is made to the change the orientation of the NI-USRP TX and RX. To ensure both devices were placed in a optimal orientation, the PSD of RSS enabled pilot signal power measurement, whilst having no objects in between the Line Of Sight (LOS) path. Apparently, a controlled environment was desired and consequently for the RCT an empty corridor space with the presence of any human, was chosen for the study. After the selection of a place with minimal environmental variations, the nominal variation of the pilot signal stabilized. The (see Fig.2) depicts the variations in RSS, which were observed in the empty space at a room temperature of 24°c, and the Fig. 3 and Fig. 4 present the observations made to TX and RX alignment patterns, and individual gain of TX and RX used during the initial testbed setup.

The optimal configuration setup ended in the setup with TX and RX gain set to 50, whilst placing both the devices at 0° with LOS as reference axis. The TX and RX are placed 2.2 meters above the ground level so that the chosen average height matches with the average height of the participants. Whereas placing the NI-USRPs at 0° with reference to the LOS showed maximum strength of pilot signal at the receiver, RSS of the pilot decreased significantly to low levels at other orientation values. For the proposed system model, a direct LOS communication link is established between the TX and RX, ensuring high RSS power level at the receiver (see Fig. 3).
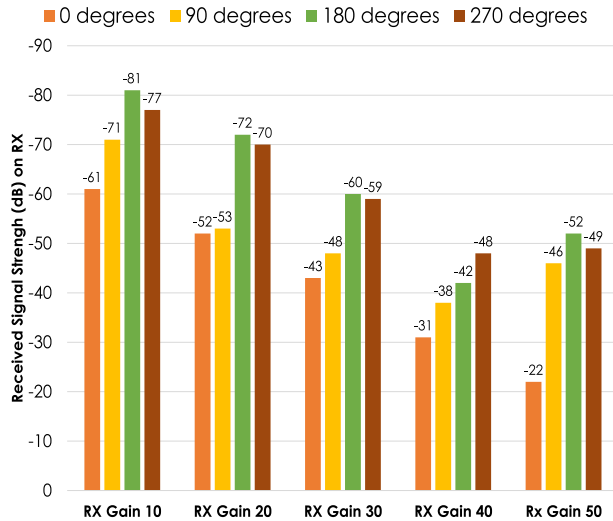
FIGURE 3. Received Signal Strength (RSS) at RX on a constant transmitter output gain of 50 db, placed at 6 meters away from RX. The RX antenna placed at an orientation of 0° with respect to the TX antenna shows the high signal strength at RX, while minimum signal strength is observed at angle of 270° of RX with respect to TX.

B. RF PILOT SIGNAL PROCESSOR APPLICATION

We build an automated RF Pilot Signal Processor (RFPSP) application in LabVIEW to record and collect RSS data. The RFPSP application output data files containing RSSI samples for each participant, who started and stopped the activity of walking in the corridor in the prescribed directions. As a result, the data of our experiment group comprised of multiple directional motion patterns pertaining to the each participant, i.e., motion from North to South (from corridor entrance to exit) and vice-versa, from East to West i.e. from RX towards TX and vice-versa, motion at an angle of 45° with right-wall as the reference axis and motion at an angle of 45° with left-wall as the reference axis.

V. DATA COLLECTION AND SYNTHESIS

Human motion data was collected in phased manner, and we employed an automated approach to our data collection process. Firstly, the NI-USRPs were setup to provide the motion data in the form of files, which were next subject to processing via the developed LabVIEW application. After processing, the LabVIEW generated prediction results, and for comparative analysis we employed similar datasets to test various other machine learning models in MATLAB. The different phases employed in the data collection process are:

A. DATA COLLECTION AND DISTRIBUTION

To enabled automated human motion data collection, we employed our RFPSP application that enabled us to collect three individual datasets for each participant. A total of 1780 samples, collected within 15 seconds duration, defined each move and for 6 directional motion patterns each dataset contained $6 \times 1780 = 10680$ RSS samples. Thus, three similar signatures (moves) of each move were prepared. Among the three, two of the datasets were used for training and third

was reserved for testing the used SNN model. Each dataset in the set of three was further partitioned into two datasets, with one designed as Training and the other as Test dataset. For the Training dataset contained 21360 data samples, including manually assigned labels to each class of motion pattern. The Test dataset containing 10680 samples only, enabled evaluation of the trained SNN model and to figure out the prediction accuracy. Since two of the three datasets were used to train the model, and only one dataset was reserved used to test, the test set contained 25% of the overall data, whereas train dataset contained 75% of the overall data.

B. DATA PRE-PROCESSING AND INCONSISTENCY CHECK

The observed Raw RSSI measurements contained noises and outliers that could significantly reduced the quality of signal describing motion signatures. Among many methods for filtering out unwanted noise, Moving Average and Median Filters offer simple solutions and are commonly adopted methods for eliminating high frequency noise components. Moving Average filter (window size of 60) is applied on the collected raw datasets of RSS, filtered out the unwanted noises and random variations. In the Moving Average and Median filters, an average or median data sample replaces a range of data points. A sliding window and multiplying factors, used provide individual weights to the averaged data samples. All datasets containing RSS samples contained random noise components. As an example, the Fig.5 and shows the raw plot signal before Moving Average filter [70] is applied and Fig.6 shows the averaged and cleansed signal after applying the filter. The collected human motion data showed data unusual variations as a result of movements, such movement of head, leaning backwards on the wall, raising hand, raising arm. These unusual movements were observed just before the data collection ended. Abreast to unwanted motion signatures,wherein redundant data as such was removed manually by padding normal RSS values in the dataset, some datasets showed missing RSS samples. As the USB type communication was used between RX and the Desktop computer, the RX setup incurred communication delays that resulted in the loss of data samples over the USB communication interface. The missing data samples were manually added using interpolation method to ensure consistency in the collected data.

- **Moving Average Filter**: The acquired human motion patterns represent both the linear and non-linear data components. We decompose the acquired time series data sequence using the Moving Average Filter (MAF), a classical method of time series decomposition [70]. An typical MAF of order D is expressed by the mathematical expression, eq(5):

$$y[i] = \frac{1}{D} \sum_{s=0}^{D-1} x[i+s] \qquad (5)$$

where $x[i]$ and $y[i]$ represent the input and output set of samples, respectively. *D* represents the number of
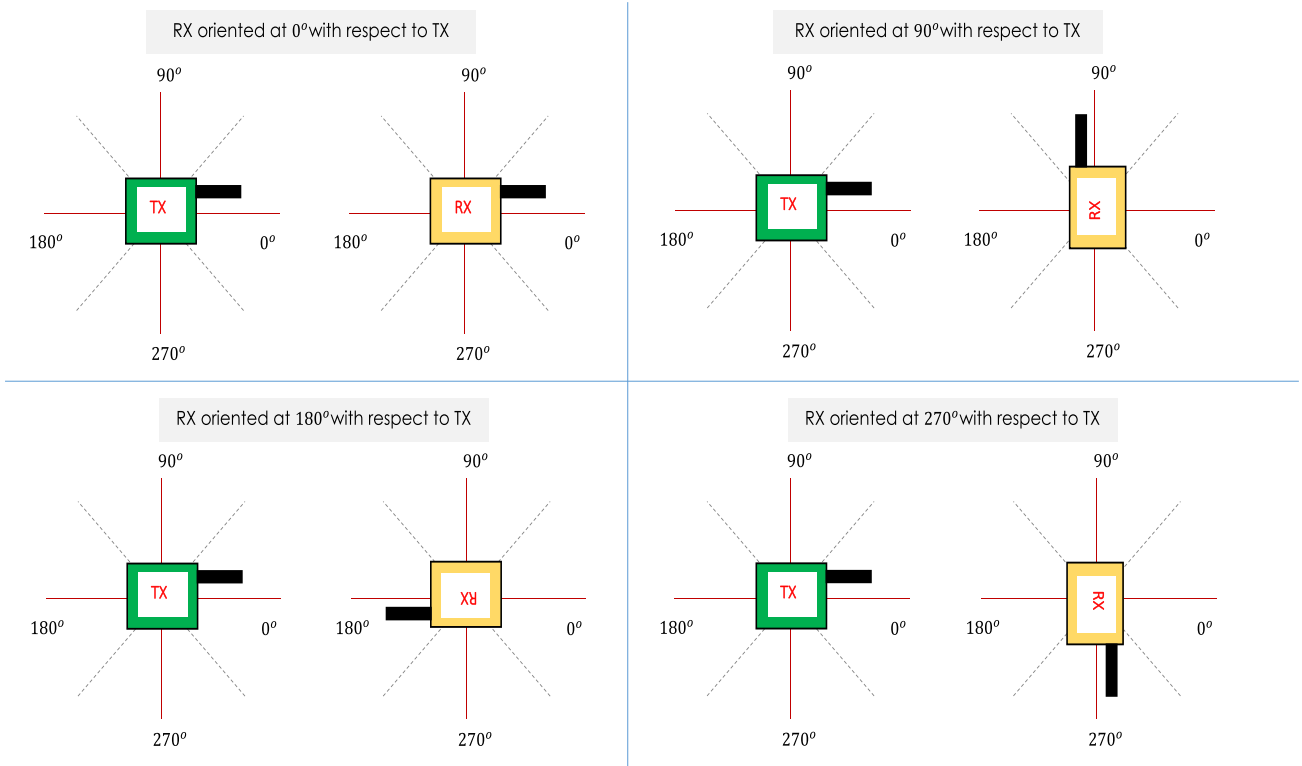
FIGURE 4. Alignment of RX with respect to TX to ensure maximum received signal strength at RX. Tx antenna orientation is static, while RX antenna orientation is tested at four angles to receive max signal strength.

samples selected for averaging. Also called as recursive form of MAF, the eq(5) can be described as a difference equation represented by eq(6):

$$y[i] = y[i-1] + x[i+p] - x[i-q] \qquad (6)$$

$$p = \frac{D-1}{2} \qquad (7)$$

$$q = p+1 \qquad (8)$$

- **Trend Elimination**: After applying MAF on the dataset of raw RSS samples, we observed the effect of trend in the filtered data. In order to remove the trends from human motion dataset, we applied the model expressed by eq(9) to detrend the time sequence data [71].

$$T[i] = T_n[i] - \frac{1}{M}\sum_{p=-k}^{k} T_n[i+j] \qquad (9)$$

where $M = 2p+1$. The trend cycle is estimated by averaging the time series with k periods of time t. The filtered data contains data samples, have data value close to each other since the averaging removes randomness in the given data. In the expression given in eq(10), the detrend sequence T_2 is the difference between the trend part of time series T_1 and the original time series T.

$$T_2 = T - T_1 \qquad (10)$$

where T is the sequence of original human motion samples; T_1 the sequence of samples representing a trend;

T_2 is the sequence of sample representing detrend in the sequence.

C. DATA PREPROCESSING

All the cleansed datasets were then prepared for ML input. With each move represented by only 1500 samples, we discarded the remaining samples for each move since few moves were missing samples. Consequently, all datasets were constrained to 1500 samples representing each move precisely for each participant. The new six moves dataset then contained 9000 samples for each dataset in a collection of three datasets for each participant. Thus, training datasets included the two datasets, with a total of 18000 samples, while the third dataset containing 9000 samples, was used to find prediction accuracy of the SNN model. All the datasets were prepared in a Comma-Separated Value (CSV) format. The training and test datasets, prepared in two CSV files, were input to the SNN based classifier that enabled prediction of direction of human motion.

VI. PATTERN DETECTION AND CLASSIFICATION

To identify human motion direction, patterns of which are hidden in the collected raw RSS data, a machine learning based solution is implemented to trace the motion signatures out of the relative datasets of each participant. Learning based algorithms are implemented as predictors in most of the recognition based applications, and typically implement Support Vector Machine (SVM) [72] for categorization.
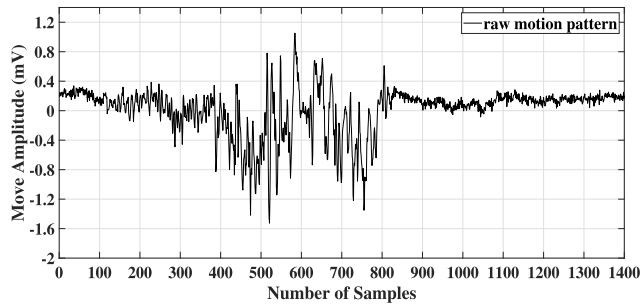
FIGURE 5. Motion signature with high frequency noise components.

FIGURE 6. Motion signature acquired after applying moving average filters.

SVMs have been mostly implemented as predictors in many studies, and these uncover embedded patterns in linear and non-linear datasets, including classification of data points that are left over from the training dataset [73]. In addition to SVM, there also exist other types of classifiers, such as K-Nearest Neighbour (KNN), Dynamic Time Wrapping (DTW), Hidden Markov Model (HMM) or Convolutional Neural Networks (CNN). While SVMs prerequisite large dataset containing support vectors that apparently determine the function of the output, SVMs are observed to be computationally expensive; hence are not reliable and may not be applicable in real-time based solutions. Furthermore, despite knowing the fact that deep learning algorithms offer high prediction accuracy, this **study leaves deep structures** since structures as such require additional parameters definitions, for instance kernel size, quantity of neurons etc, whilst having many layers of hidden neuron that complicate the overall architecture of the algorithm. However, SNNs can be used on mobile devices and offer more light weight architecture than other types of classifiers. Therefore, this study implements Shallow Artificial Neural Networks as a machine learning based solution since ANNs outperform SVMs in terms of computational efficiency [58], [74], [75].

A. SHALLOW NEURAL NETWORK (SNN)
ANN algorithms mimic the neural system functions of living organisms, and typically implement fully connected computational units called neurons. ANN organizes these neurons in different layers, wherein the first layer is called as the input layer, the second containing few hidden layers, and the third layer called as is the output layer. Among the three layers, output of each hidden layer feeds the input of the next layer. This study employs a single hidden layer SNN as the machine learning solution to recognize the directional patterns in human motion data. Fig.7 shows a SNN that includes n inputs, d hidden neurons placed in a single hidden layer, and a only one output layer y. SNN model defines the input-to-output relation as a function, $f : \mathbb{R}^n \to \mathbb{R}$ that associates the input vector $x \in \mathbb{R}^n$ to a scalar based on the following relationship, eq(11):

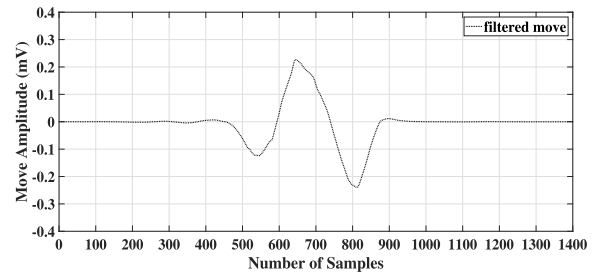$$x \to f_{v,W}(x) := \sum_{n=1}^{d} v_l \xi(\langle w_l, x \rangle) \qquad (11)$$

where $w_l \in \mathbb{R}$ represent vector with edge weights that associate input to hidden node lth and $v_l \in \mathbb{R}$ represents edge weight connecting the hidden node lth to the output layer. The expression $\xi : \mathbb{R} \to \mathbb{R}$ is the activation function used for the each hidden node in the hidden layer. The matrices $w \in \mathbb{R}^{d \times x}$ and $v \in \mathbb{R}^d$ represent a compact notation of the weights w_l/v_l, eq(12):

$$W = \begin{bmatrix} w_1^T \\ w_2^T \\ \vdots \\ w_k^T \end{bmatrix} \quad v = \begin{bmatrix} v_1 \\ v_2 \\ \vdots \\ v_m \end{bmatrix} \qquad (12)$$

The cost function of a given Fully Connected Neural Network (FCNN) [76]. The network has d units organized in a single hidden layer, and includes the linear output unit that computes sum-of-squares error for the given set of input data expressed by eq(13):.

$$\sum_{m=1}^{l} \frac{1}{2}(f_{FCNN}(x_i) - y_i)^2 \qquad (13)$$

where

$$f_{(FCNN)}(x) = c_0 + \sum_{p=1}^{Q} \gamma_k \psi(\omega_k, x) \qquad (14)$$

In the eq(14):, $\{\omega_k\}_{p=1}^{Q}$ denotes the weights of the hidden layer and $\{\gamma_k\}_{p=1}^{Q}$, the weights of output layer. The expression $\psi(c, \omega, x)$ represents the sigmoidal for Multilayer Perceptrons (MLPs) as the activation function for the hidden units.

B. FEATURE EXTRACTION
With current testbed, only a single vector containing a stream of RSS samples corresponding to each move is collected. SNN algorithm requires more features vectors for effectively classifying the direction of moves. Thus, additional feature vectors based on the dynamic non-periodic signal properties were formulated. The extracted feature vector space consisted of RSS variations and associated radio signal properties for each participant observed in six directions. The properties included various signal properties such as mean $\bar{x}$, standard deviation (sd), difference d, variance σ, and signal energy over the sampling interval. The directional
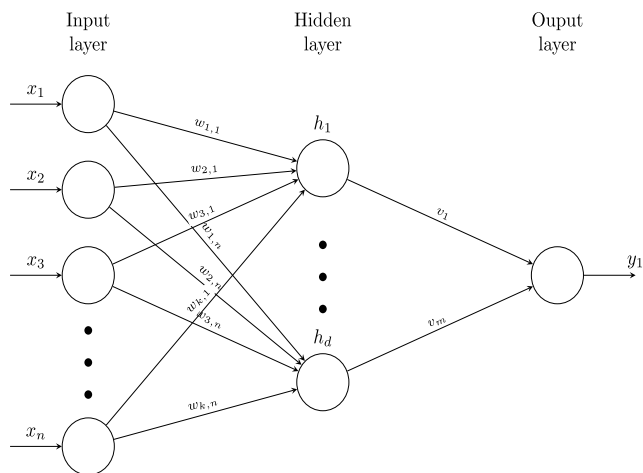
FIGURE 7. A Shallow Neural Network (SNN) with a single hidden layer.

motion datasets (see eq(15)) for each of the four participants were collected and class labelled each move of the six associated moves as 1,2,3,4,5 and 6 respectively. Here the superscripts are indexes representing each participant, and subscripts are indexes that denote the collected data points. The input to the SNN algorithm is a matrix of the form shown expression eq(16):

$$(s_u^1, q_r^1), (s_u^2, q_r^2), (s_u^3, q_r^3), and(s_u^4, q_r^4) \qquad (15)$$

$$
\begin{pmatrix}
(s_{1,1}^1) & (s_{1,2}^1) & (s_{1,3}^1) & \cdots & (s_{1,n}^1) & \rightarrow (q_1^1) \\
\vdots & \vdots & \vdots & \vdots & \vdots & \vdots \\
(s_{u,1}^1) & (s_{u,2}^1) & (s_{u,3}^1) & \cdots & (s_{u,n}^1) & \rightarrow (q_6^1) \\
(s_{1,1}^2) & (s_{1,2}^2) & (s_{1,3}^2) & \cdots & (s_{1,n}^2) & \rightarrow (q_1^2) \\
\vdots & \vdots & \vdots & \vdots & \vdots & \vdots \\
(s_{u,1}^2) & (s_{u,2}^2) & (s_{u,3}^2) & \cdots & (s_{u,n}^2) & \rightarrow (q_6^2) \\
(s_{1,1}^3) & (s_{1,2}^3) & (s_{1,3}^3) & \cdots & (s_{1,n}^3) & \rightarrow (q_1^3) \\
\vdots & \vdots & \vdots & \vdots & \vdots & \vdots \\
(s_{u,1}^3) & (s_{u,2}^3) & (s_{u,3}^3) & \cdots & (s_{u,n}^3) & \rightarrow (q_6^3) \\
(s_{1,1}^4) & (s_{1,2}^4) & (s_{1,3}^4) & \cdots & (s_{1,n}^4) & \rightarrow (q_1^4) \\
\vdots & \vdots & \vdots & \vdots & \vdots & \vdots \\
(s_{u,1}^4) & (s_{u,2}^4) & (s_{u,3}^4) & \cdots & (s_{u,n}^4) & \rightarrow (q_6^4)
\end{pmatrix}
$$

$$(16)$$

The subset $s_{1,1}^z \times s_{u,n}^z$ is a partial-matrix representing manually extracted radio signal properties from RSS for the participant s^1 with assigned label vector q_1^1 to q_6^1, categorize every move of comprising 1500 RSS samples. With each move of $s_{1,1\rightarrow n}^1$ to $s_{1500,1\rightarrow n}^1$ is associated a move label q_r^1. The other three participants' feature vectors $s_{1,1}^2$ to $s_{u,n}^2$, $s_{1,1}^3$ to $s_{u,n}^3$ and $s_{1,1}^4$ to $s_{u,n}^4$ are assigned class labels q_r^2, q_r^3 and q_r^4 respectively. The superscript $z : 1 \rightarrow 4$ denotes the participant index. The subscript u is an index of the samples that range from $u : 1 \rightarrow 9000$ for each of the subset matrix for each participant, while $r : 1 \rightarrow 6$ represents index of the six directional movements undertaken by the subjects.

C. DEFINING FEATURE VECTORS

The number of features to be defined for the motion classification is determined by signal itself. Since this study employs a single carrier component, the directional motion signature pattern is determined by signal amplitude, embedding motion characteristics in the form of signal variations over time. With the inspiration from [77] to uniquely identify each motion pattern, we construct a set of manually crafted features from the RSS of pilot signal. The manually crafted feature vector set considers **six different features** of the received signal pattern, so as to address signal characterization properties that include mean, standard deviation, skewness, Real-Signal Kurtosis (RSK), average power, and energy of motion signalling period, wherein each received signal, with a signal sample z of the RSS signal, consists of 1 by η data samples. Following are the expressions, eq(17,18,19,20,21,22,23), used in this study to manually craft the six possible feature vectors that distinguish each motion pattern uniquely.

- **Mean** (μ) – Mean [78] is an average value of time varying signal, and it is computed over a period of time. μ is expressed by the eq(17), is an "equivalent" constant level, represents the same area as the signal over the same time:

$$\mu(z) = \frac{1}{\eta}\sum_{p=0}^{\eta-1} z(p) \qquad (17)$$

- **Standard deviation** (σ) – Standard deviation [78] provides a measure of spread of the amplitude values and indicates the width of the bell curve for a Gaussian noise signal or a given signal and is expressed by eq(18):

$$\sigma = \sqrt{\frac{1}{\eta-1}\sum_{p=1}^{\eta} \{z(p) - \mu(z)\}^2} \qquad (18)$$

- **Skewness** (γ) – skewness (I/Q) [79] is a higher-order statistical attributes of a time series. Skewness reveals the symmetry in the estimated probability density function (PDF) of the signal amplitude. γ is expressed by eq(19):

$$\gamma = \frac{E\{z(p) - \mu(z)\}^3}{\sigma^3} \qquad (19)$$

- **Real-Signal Kurtosis** (RSK) – is proposed by [78] and provides estimate of kurtosis of In phase and Quadratic (I/Q), components of the signal. Kurtosis is given by eq(20).

$$\kappa = \frac{E\{z(p) - \mu(z)\}^4}{\sigma^4} \qquad (20)$$

Averaging the estimated kurtosis components (I/Q), determines the RSK feature, which is
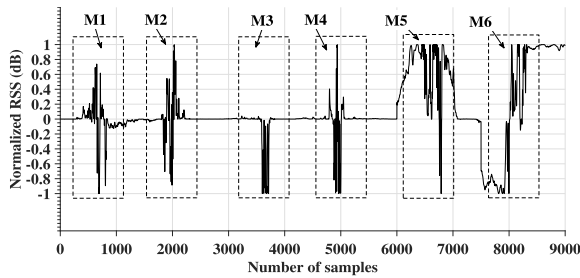
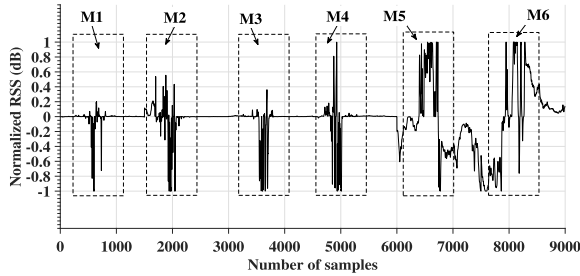**FIGURE 8.** Six directional motion patterns of P1 as input to the SNN model.

FIGURE 9. Six directional motion patterns of P2 as input to the SNN model.

FIGURE 10. Six directional motion patterns of P3 as input to the SNN model.

FIGURE 11. Six directional motion patterns of P4 as input to the SNN model.
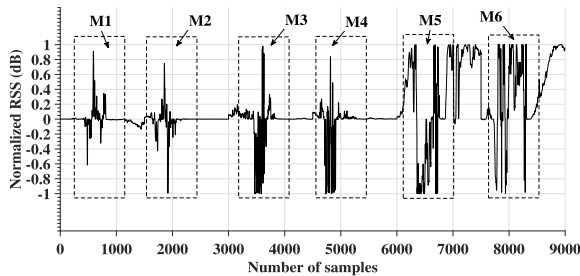

FIGURE 12. All 24 directional motion patterns as input to the SNN model.

which is available in LabVIEW application suite, to precisely estimate the accuracy levels of available SNN models, whilst aiming to achieve high performance. Multiple iterations on 12 different neuron counts concluded in the selection of the optimized SNN model (see Fig.19). The SNN model was created for each participant to individually check model accuracy for each of the six movies, and also created was an overall model that trained on all 24 moves of the four different subjects, so as validate the overall accuracy of the SNN model on a aggregated dataset. Figures 8 to 11 show the individual unique motion patterns of each participant, whereas Fig. 12 shows an outcome of the combined move set.

An SNN type classifier was configured and implemented using evaluated optimized settings for each of the participants. The SNN type classifier was input a dataset in the CSV file format that contained identified feature vectors and the associated class labels. After the SNN tuning parameters were set to the optimal settings, the classification accuracies observed during the tuning parameter optimization and actual training, remained almost the same. For the actual training With optimized tuning parameter selections, the model prediction accuracies remained exactly the same as observed during the search for optimized model parameters. The average model training accuracy for each participant depicted a near classification accuracy of 93%, whereas the training accuracy of the overall SNN model just resulted in an accuracy of 74.5%.

E. TESTING SNN MODEL

The preprocessed test data set was split up into individual datasets corresponding to each of the four participants, including a combined dataset of all four, for the purpose of testing the developed SNN model. Each individual data

expressed by eq(21):

$$RSK = \frac{\left|Kurtosis_{(I)}\right| + \left|Kurtosis_{(Q)}\right|}{2} \quad (21)$$

- **Average Power** – average power [80] of a discrete time periodic signal over its length is given by the relation. Average Power is expressed by eq(22):

$$AveragePower = \lim_{K \to \infty} \frac{1}{2K+1} \sum_{\eta=-K}^{K} |z(\eta)|^2 \quad (22)$$

- **Energy** – energy [80] of each signal over its length is given by the relation:

$$Energy = \sum_{\eta=-\infty}^{\infty} |z(\eta)|^2 \quad (23)$$

D. TRAINING SNN MODEL

SNN model performance measurements were carried out with the datasets, split into training and test dataset. The SNN model was tuned with the random optimization program,
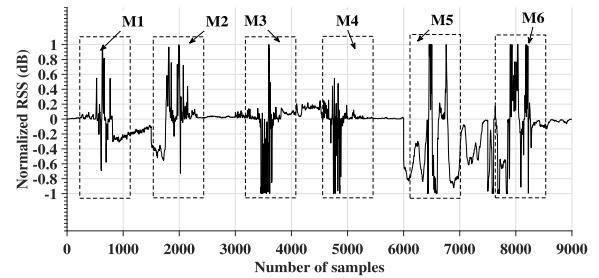
FIGURE 13. Confusion matrix: SNN model on combined test dataset of all four participants with Predicted labels. True class presents actual directional moves, and the Predicted Classes represent detected moves.

TABLE 3. Labels and semantic.

Participant	Gender			
P1	Male	M1	North to South
P2	Male	M2	South to North
P3	Female	M3	West to East
P4	Male	M4	East to West
		M5	North-West to South-East at 45°
		M6	North-East to South-West at 45°

set consists of proposed feature vectors of six directional motion patterns of the each participant. In light of an overall data set and individual datasets, we developed individual SNN models that were trained on each participant individual data set, and an overall SNN model that was trained on the combined dataset of all the four participants. Next, the each individual test data set, having sequentially arranged data of six different moves of each participant, was input to the SNN classifier to evaluate the models' accuracy. The individual test set contained 9000 samples, including associated class labels for each directional move. Furthermore, we input the overall test dataset that contains all 24 directional move patterns of four participants to the SNN classifier, which we name as an "overall SNN model". Figures 14 to 17 show the actual and predicted outcomes of individual models, whereas Fig. 13 shows an outcome of the overall SNN model, used to find direction of motion of all the four participants.

VII. RESULTS AND ANALYSIS

The two NI-USRP 2921 TX/RX devices,which were installed in two adjacent rooms, separated by a distance of 6 meter, established a communication transmitter-receiver

FIGURE 14. Confusion matrix for test dataset of P1.

pair. During the experiment, our proposed testbed setup showed instability in the received signal strength because of unwanted activities by human in the corridor. The pilot signal's dynamic nature showed little instability due to mobile devices that were carried by the humans in the room with RX. The NI-USRP RX device enabled us to observe the normal transmission of pilot in the corridor area, and as the RF pilot signal presents a highly dynamic and sensitive nature, we observed considerable variations in the received signal strength with little human body movements, which include turning around, leaning on the wall, making gestures with hand, etc. To ensure that our data collection excluded such variations, the testbed environment was limited to the participant only, and with absence of other human movements, except the motion executed by the subject(s) under investigation, enabled least variations in RSS of pilot signal. Fig. 2 shows the six recorded pilot signal strength variations under no human movement. Fig. 2 depicts dynamic variations in pilot RSSI at room temperature. The random variations
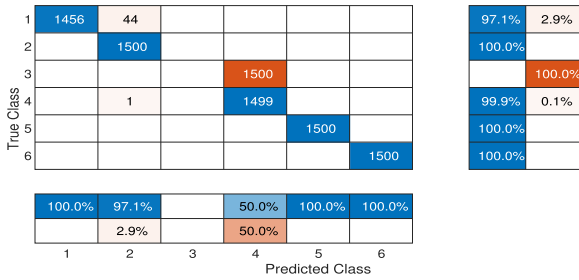
FIGURE 15. Confusion matrix for test dataset of P2.

FIGURE 16. Confusion matrix for test dataset of P3.

FIGURE 17. Confusion matrix for test dataset of P4.

FIGURE 18. SNN performance evaluation on individual test sets.

expression given in eq(24):

$$precision = \frac{T_P}{T_P + F_P} \qquad (24)$$

where T_P and F_P denote the true positive and false positive values, respectively.

The Recall evaluation parameter quantifies sensitivity, and is given by the eq(25):

$$recall = \frac{T_P}{T_P + F_N} \qquad (25)$$

where F_N denotes the false negative value.

The weighted average of recall and precision is known as F-measure, and it is quantifies the weighted average using following expression given in eq(26):

$$F1 = \frac{precision \, recall}{precision + recall} \qquad (26)$$

where F_1 denotes the false negative value.

VIII. PERFORMANCE EVALUATION – SINGLE VERSUS MULTIPLE SNN MODELS

We evaluated the training and test datasets using SNN algorithm, the accuracies observed during SNN training and testing varied drastically. Testing SNN on individual datasets resulted in prediction accuracies ranging between 80% to 83%, whereas testing SNN on the overall data set results in just 75%-78%.

A. TRAINING AND TESTING INDIVIDUAL SNN MODELS

LabVIEW application was used to build, train and test the SNN models. With individual models, trained to predict accuracies of more than 85% resulted in overfitting, and as a result of computing the prediction accuracy on the test datasets, reduced nearly to about 30% to 40%. After several attempts, we trained our individual SNN models to predict training accuracies ranging between 80%-85% that finally resulted in best fit. These best fit models actually showed an increase in the actual prediction accuracy of each model, with accuracy of nearly 83%. Moreover, to ensure that the four models could identify each participant uniquely, we conducted as

of pilot having -35 dBm to -38.5 dBm approximate strength was observed even in absence of human movements, and this clearly shows the variability of the RSS. However, when each of the participant performed the activity of walking though the corridor path, the dynamics of RSS showed huge variations that eventually resulted in a pilot signal with embedded unique motion patterns. The patterns embedded in the RSSI of the pilot hold the unique motion patternstyle of the participant(s). Thus, the unique sensitive pattern detection system can be categorized as a highly sensitive motion recognition system since even a micro moment gets embedded in the pilot. When the motion patterns are subject to analysis, the study results reveal the sensitive critical information contained in RSSI dataset, could be systematically explore to identify unique direction motion patternssignatures of any person.

A. PERFORMANCE METRICS

We use measurement parameters - precision, recall, and F-measure metrics to evaluate the proposed models of human motion direction prediction [81]–[83]. The precision parameter is a positive value that quantifies the prediction results of a classification process. It is computed by the following
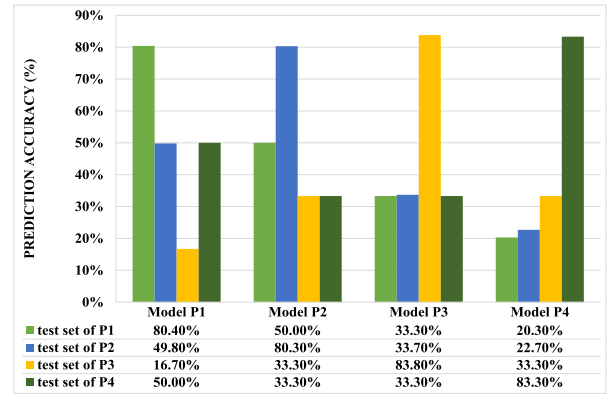
FIGURE 19. SNN training and testing performance evaluation.

FIGURE 20. Narrow Neural Network (NNN) configuration settings in MATLAB [84].

cross validation test. Figure 18 shows the cross validation of models along with the observed motion direction prediction accuracies. Each model is tested against all the four individual datasets. In each individual test that resulted in a motion direction predicted outcome, each SNN model showed wrong predictions of moves 3 and 4 that correspond to the moves – from West to East, and vice-versa, while rest of the directional motion patterns were detected with almost 100% accuracy.

B. TRAINING AND TESTING AN OVERALL SNN

For the training of SNN on an overall dataset resulted in higher prediction accuracies reaching almost 82%. With the accuracies observed during training sequence, the test set accuracies varied for neurons less than $x - inputs$ and greater than 96. However, when the overall model was trained to an accuracy level ranging between 75%-78% using neuron count greater than $x - inputs$ and less or equal to 96, the test accuracies remained almost constant at 70% (See Figure 19).

IX. COMPARATIVE ANALYSIS

To compare and trace out the best prediction model that detects the direction of human motion precisely, we trained and tested various other ML models available in MATLAB. We employed Decision tree algorithms, Linear Discriminant Analysis (LDA), Naïve Bayes, SVMs, and KNN algorithms to test our proposed model, which resulted in contrasting prediction accuracies. Tables – 5, 6 and 7 show the observed results of these various machine learning models. Our observation of the collected results reveal that KNN outperformed the rest of the models. However, the Shallow Neural Network (SNN) based prediction model showed the highest prediction results compared to the rest of the models.

The KNN seems to compete equally well with the SNN, whilst showing a consistent motion direction prediction accuracy of approximately 83% on the individual test set, and 71% accuracy on the overall data set of the three male participants. However, it should be noted that the **KNN just showed a motion direction prediction accuracy of 67% only on the individual test data set of the female participant (P3)**. Although this fact is not investigated yet, in the future studies this unusual behaviour needs further research. Therefore, a study on the gender based motion detection system is imperative.
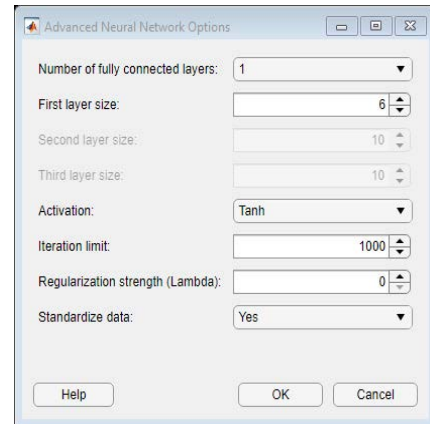
For the rest of models, showed varying results and no consistency in human motion direction classification. The Decision Tree based models revealed the varying prediction accuracies on the individual datasets and 50%-60% prediction accuracies on overall datasets. Similar to Decision tree type models, Naive Bayes type models showed a consistent accuracy of 50-60% on overall data set, whilst failing to maintain the consistency on individual datasets. On the other hand, LDA showed a minimal improvement in the accuracy that ranged between 60% to 70% on average. Although SVMs are best suited for the classification of non linear data entities, SVM models employed in the study revealed 67% average accuracy on individual datasets and 71% on overall datasets only.

Overall, the models based on KNN show better prediction accuracies than others, however fails to compete with a single hidden layer neural network.

A. CROSS-VALIDATION OF SHALL NEURAL NETWORK MODELS

Cross-validation technique assesses and evaluates machine learning algorithm's performance. Generated datasets are input to machine learning algorithm to assess the model's performance, and with unknown datasets as input to an algorithm, allows assessment of prediction outcomes. Assessment techniques require random partitioning of a given dataset into a number of training and testing datasets. During several iterations, training sets train a supervised learning algorithm, while a single testing dataset is reserved during each iteration to test accuracy of model.

A commonly used Common Cross-Validation Technique called **k-fold** method, partitions a given dataset into k folds (random subsets) of nearly equal sizes. k-folds consist of k-1 subsets reserved to train a machine learning algorithm and one test subset that evaluates the trained machine learning model's performance. To assess the model's performance, the process iterates ω times to generate a new single subset (test set) for validation. Average estimation error across all k partitions is typically expressed by ϵ.
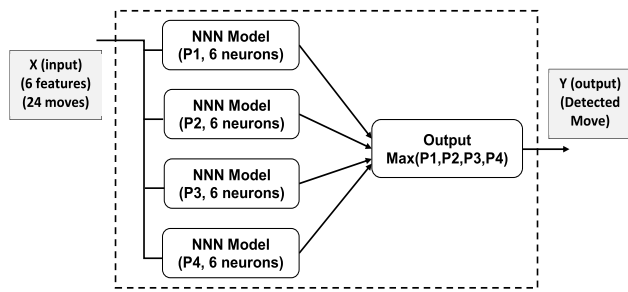
FIGURE 21. Ensemble model of combined four Narrow Neural Network (NNN) models.

FIGURE 22. Overall model based on Narrow Neural Network (NNN).

TABLE 4. Results of paired-sample t-Test at significance level of 5%. Model-1 and Model-2 represent the overall SNN and Ensemble SNN model, respectively.

	Model-1	Model-2
Mean	0.74024	0.89129
Variance	0.00054	0.00119
Observations	1000	1000
Pearson Correlation	-0.03590	
Hypothesized Mean Difference	0.00000	
df	999	
t Stat	112.98751	
P(T<=t) one-tail	0.00000	
t Critical one-tail	1.64638	
P(T<=t) two-tail	0.00000	
t Critical two-tail	1.96234	

This study employs **5-fold** Cross-Validation method to partition dataset into 5 equal folds of nearly equal sizes. The Cross-validation is configured at an iteration count of $\omega = 1000$. To perform comparative analysis and cross validate the developed models, comparative analysis of two model is carried out using MATLAB [84]. Narrow Neural Network (NNN) is a form of SNN available in MATLAB, and the NNN model can be trained and tested using customized parameters. Since the input layer of the individual training models see 6 features, each NNN model's first layer is set with 6 neurons, and four such individual models are trained and tested for four different participants.

Although each model is trained and tested individually, the ensemble model containing four models with a common input, results in class probability as a common output of all the four. Each individual classifier has *Tanh* as activation function at its output, and the probabilities of each model are fed to objective function $max(P_1, P_2, P_3, P_4)$. The objective function outputs the class of identified direction having maximum estimated probability by the objective function (see Fig. 21).

Compared to ensemble model, the overall model also sees the same directional moves of four different participants at input. Thus, the input needs to have 24 neurons to classify $6 \times 4 = 24$ moves. NNN is configured with an input layer of 24 neurons and an iteration count of $\omega = 1000$. **5-fold** Cross-Validation again evaluates the performance of the overall model for comparison to the Ensemble model. Fig. 22) shows the block diagram of overall model with 6 input feature vector X, and 24 directional classifications at output Y.

B. HYPOTHESIS TEST

To test the statistical significance of our proposed models, the study proposes the following two hypothesis, and applies Paired t test to compute statistical parameter t and probability P.

H_0 : the population mean of differences between observed ML model accuracies of Ensemble (NNN model) and overall model is zero, $H_0 : \mu_d = 0$.

H_1 : the population mean of differences between observed ML model accuracies of Ensemble (NNN model) and overall model is not equal to zero. $H_1 : \mu_d \neq 0$. $\alpha = 0.05$ is the level of significance:
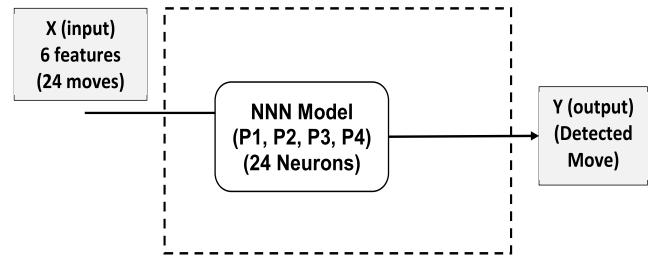
1) PAIRED T TEST

t test [85], a statistical analysis technique, is also known as Student's t test. t test is applicable to one sample only or two samples with the difference in between their two independent means. t test reveals the statistical difference that may exist between two independent sample means or within a sample mean. However, difference between two samples is close to zero if the sample means are same, and additional statistical tests may be applied on data to find out the statistical significance between the variables.

Paired t test statistically tests the difference between two paired results of a sample. The resulting difference between two paired samples is close to zero, if applied treatments on the two samples are same, and computed differences between the sample means used during the test result in a difference of 0.

The variance of the difference of two variables, for example, A and B, $Var(A - B)$, is expressed by the equation eq(27) [85],

$$Var(A - B) = \sigma_1^2 + \sigma_2^2 - 2\rho\sigma_1\sigma_2 \qquad (27)$$

where σ_1^2 and σ_2^2 represent the variance of variables A and B, respectively. ρ represents the correlation coefficient for the two variables. Correlation coefficient ρ equals to 0 for two independent groups used in an independent t test, and the sum

TABLE 5. k-nearest neighbors algorithms.

	KNN Fine	KNN Medium	KNN Coarse	KNN cosine	KNN cubic	KNN Weighted
P1-Train	92%	91%	90%	91%	91%	92%
P1-Test	83%	83%	84%	87%	83%	83%
P2-Train	100%	100%	98%	100%	100%	100%
P2-Test	83%	83%	84%	87%	83%	83%
P3-Train	100%	100%	99%	100%	100%	100%
P3-Test	67%	67%	69%	69%	67%	67%
P4-Train	100%	100%	99%	100%	100%	100%
P4-Test	83%	83%	68%	68%	83%	83%
All-Train	98%	98%	96%	98%	98%	98%
All-Test	74%	74%	73%	57%	74%	74%

TABLE 6. Decision tree, linear discriminant analysis, and naive bayes algorithms.

	Tree (Fine)	Tree (Medium)	Tree (Coarse)	Linear Discriminant Analysis	Naïve Bayes (Gaussian)	Naïve Bayes (Kernel)
P1-Train1	92%	92%	75%	75%	91%	92%
P1-Test	50%	50%	67%	67%	57%	67%
P2-Train	100%	100%	83%	75%	100%	100%
P2-Test	50%	50%	67%	67%	57%	67%
P3-Train	100%	100%	83%	100%	92%	99%
P3-Test	67%	67%	50%	67%	60%	50%
P4-Train	100%	100%	83%	100%	99%	100%
P4-Test	83%	83%	83%	83%	83%	83%
All-Train	98%	75%	21%	81%	93%	98%
All-Test	58%	50%	13%	54%	52%	54%

TABLE 7. Support vector machine algorithms.

	Linear SVM	Quadratic SVM	cubic SVM	Fine Gausian SVM	Medium Gaussian SVM	Coarse Gaussian SVM
P1-Train1	92%	92%	92%	92%	92%	83%
P1-Test	67%	67%	83%	66%	67%	67%
P2-Train	100%	100%	100%	100%	100%	100%
P2-Test	67%	67%	83%	66%	67%	67%
P3-Train	100%	100%	100%	100%	100%	100%
P3-Test	67%	83%	49%	83%	67%	67%
P4-Train	100%	100%	100%	100%	100%	100%
P4-Test	83%	83%	67%	83%	83%	67%
All-Train	96%	98%	98%	diverges	diverges	96%
All-Test	71%	50%	54%	0%	0%	63%

of the two variances represents the variance of the difference between the two variables.

However, ρ may or may not be equal to 0 for paired variables. Apparently, t statistic is different for the two dependent samples and the expression equation eq(28) is represents a modified form of equation eq(27) for the paired number of samples.

$$t = \frac{\bar{\chi}_1 - \bar{\chi}_2}{s_{(1+2)}\sqrt{\frac{1}{n_1} + \frac{1}{n_2}}} \qquad (28)$$

where $\bar{\chi}_1$ and $\bar{\chi}_2$ represent the sample means of two variables A and B. Variable s represents sample variance, expressed by equation eq(29). To determine the sampling distribution of the mean, sample variance is used instead of the

population variance [85]:

$$s^2 = \frac{\sum (x_i - \bar{x})^2}{n - 1} \qquad (29)$$

Here x_i represents data sample at index i; $\bar{x}$ represents sample mean, and $n_1 = n_2 = n..$ The expression $s_1^2 + s_1^2 - 2\rho s_1 s_2$, computes statical variance between the two variables and takes into account the correlation coefficient ρ. As a result, t statistic in a paired t test is given by the equation eq(30):

$$t = \frac{\bar{X}_1 - \bar{X}_2}{s_{(1+2)}\sqrt{\frac{s_1^2 + s_1^2 - 2\rho s_1 s_2}{n}}} \qquad (30)$$

In equation eq(30), for the correlation coefficient $\rho > 0$, t statistic increases as the denominator becomes smaller.

Subsequently, statistical power of paired t test increases compared to an independent t test. On the other hand, for the correlation coefficient $\rho < 0$, statistical power decreases and lowers compared to the independent t test.

This study applies t test, and the observations of Ensemble NNN and overall model substitute the samples *A* and *B* introduced in the prior section.

The test statistic is $t = 112.987$, with 999 degrees of freedom, and $P < 0.0000$ (reported up to four decimals only). Since observed p-value is less than $\alpha = 0.05$, the study rejects the null hypothesis and concludes that there is a significant difference between the proposed ML models having mean validation accuracies of 74.02% (for overall model) and 89.13% (for Ensemble NNN model) approx. for prediction of human motion direction, respectively. The test clearly shows that Ensemble model can offer high prediction accuracy to determine direction of human motion using RSS.

C. OVERALL ANALYSIS AND RESEARCH DIRECTIONS

Our analysis on observed results shows that individually trained models for recognizing unique signatures (directional moves) of each participant provides higher prediction accuracies than the overall trained model for all four participants. This leads us to conclude that in a scenario with n-participants, n-models can be built to ensure that the proposed system delivers higher accuracy in predicting the individual signatures (directional moves). However, this demands distributed processing platforms, wherein at *n*-node located at *m* locations can each hold a pre-trained model. Upon receiving a common input (a sample set of moves of a person) over a communication network, these individual nodes can output predictions. The node with the highest predicted score will enable the identification of the move along with the identity of the person. Distributed processing systems as such would require nodes having embedded devices, like FPGA based platforms, supporting and running machine learning algorithms for higher efficiency. In continuation of this study, implementation of a newly proposed distributed processing system model is aimed in the next study, wherein delivery of results showing real time performance of distributed embedded systems employing machine learning algorithms is expected, including network performance measurements.

D. ADDITIONAL TESTBED REQUIREMENTS

While the human motion patterns were observed via an automated system application, USRPs posed problems that related to clock synchronization. The USRP radio device configured as RX, encountered latency, including drift in the received pilot signal. The system attempted to detect directional locomotion patterns within a microsecond time duration that required very high speed communication interface between the USRP and the Desktop Computer. Similarly, due to local oscillator frequency mismatch between the TX and RX, the pilot signal appearing on the RX, was offset by a frequency of 4KHz. The USRP sampling rate of RX device to manually calibrated during the testbed optimization process. The frequency offsets have been often reported in the USRP

devices [86], and to calibrate the TX and RX device properly, an external reference clocks signal generator is prerequisite to further studies. Hence frequency offsets in received pilot signal can be stabilized by using same reference clock signal for both the RX and TX. The process of finding optimized tuning parameters during the initial testing and calibration phase helped to establish an accurate and efficient testbed. The calibration parameters that results in the correct tuning of the testbed included power, sampling frequency, pilot signal frequency, distance and receiver orientation.

X. CONCLUSION

This study focused on the identification of direction of human motion prevailing behind the walls, using RSS of a pilot radio carrier and Shallow Neural Network. The study implemented proposed a system model and a testbed, employing state-of-the-art SDRs, to collect and analyze human motion patterns in indoor environments. The results of this study show that the use of RSS, embedding human motion patterns and application of SNN to classify such embedded motion patterns in RSS data, recognizes and predicts the direction of human motion with 89% approx. at 1000 iterations detection accuracy, however, using individual data models trained on each subjects motion datasets. The study also provides a comparative analysis of various machine learning models that were trained on the collected data, with prediction results showing that KNN can also help in prediction of human motion, however, the accuracy is lower than the SNN based prediction models. The proposed system model can be reproduced and validated on any commercially available SDRs for further research. A feature vector set has been proposed as input to the SNN model. The NI-USRP 2921 SDR model implemented was implemented, which enabled fine tuning of both the transmitter and receiver designs, so as to collect the directional human motion data.

In the future studies, RSS would be employed to precisely localize and detect human identity, as well as gender, walking behind the walls in given indoor or outdoor environment. A real time motion recognition system is anticipated based on a distributed processing model. This would enable processing of each subjects data on an individual processing unit connect to the distributed processing system. To design the new distributed processing testbed, it is envisioned to interface multiple SDRs, as individual radio units, interfacing high speed desktop computers. Each desktop computer would be running an application to implement SNN model trained on a specific subject. This would allow real time comparison of inputs received from multiple SDR units in real time. Further research in current study would guide researchers in developing real-time monitoring gadgets or apparatus and also to test and evaluate system performances in other available ISM bands. Moreover, it will lead researchers to develop more efficient, robust, and highly accurate HMRs if FPGA based processing units or cloud services are employed for high speed designs, since these offer more flexibility for modular design and prototyping.

REFERENCES

[1] K. Hu, J. Ye, E. Fan, S. Shen, L. Huang, and J. Pi, "A novel object tracking algorithm by fusing color and depth information based on single valued neutrosophic cross-entropy," *J. Intell. Fuzzy Syst.*, vol. 32, no. 3, pp. 1775–1786, Feb. 2017.

[2] J. Liu, G. Teng, and F. Hong, "Human activity sensing with wireless signals: A survey," *Sensors*, vol. 20, no. 4, p. 1210, Feb. 2020.

[3] M. Smith and S. Miller, "Correction to: The ethical application of biometric facial recognition technology," *AI Soc.*, pp. 1–9, Jul. 2021.

[4] Y. Wang, S. Wang, M. Zhou, Q. Jiang, and Z. Tian, "TS-I3D based hand gesture recognition method with radar sensor," *IEEE Access*, vol. 7, pp. 22902–22913, 2019.

[5] E. V. Añazco, S. J. Han, K. Kim, P. R. Lopez, T.-S. Kim, and S. Lee, "Hand gesture recognition using single patchable six-axis inertial measurement unit via recurrent neural networks," *Sensors*, vol. 21, no. 4, p. 1404, Feb. 2021.

[6] K. Qian, C. Wu, Z. Zhou, Y. Zheng, Z. Yang, and Y. Liu, "Inferring motion direction using commodity Wi-Fi for interactive exergames," in *Proc. Conf. Hum. Factors Comput. Syst.*, May 2017, pp. 1961–1972.

[7] P. Huang, X. Zhang, S. Yu, and L. Guo, "IS-WARS: Intelligent and stealthy adversarial attack to Wi-Fi-based human activity recognition systems," *IEEE Trans. Dependable Secure Comput.*, early access, Sep. 8, 2021, doi: 10.1109/TDSC.2021.3110480.

[8] S. Feng, H. Shi, L. Huang, S. Shen, S. Yu, H. Peng, and C. Wu, "Unknown hostile environment-oriented autonomous WSN deployment using a mobile robot," *J. Netw. Comput. Appl.*, vol. 182, May 2021, Art. no. 103053.

[9] W. Wang, A. X. Liu, M. Shahzad, K. Ling, and S. Lu, "Device-free human activity recognition using commercial WiFi devices," *IEEE J. Sel. Areas Commun.*, vol. 35, no. 5, pp. 1118–1131, May 2017.

[10] S. A. Bhat, A. Mehbodniya, A. E. Alwakeel, J. Webber, and K. Al-Begain, "Human motion patterns recognition based on RSS and support vector machines," in *Proc. IEEE Wireless Commun. Netw. Conf. (WCNC)*, May 2020, pp. 1–6.

[11] Z. Liu, X. Ruan, and J. He, "Efficient 2-D DOA estimation for coherent sources with a sparse acoustic vector-sensor array," *Multidimensional Syst. Signal Process.*, vol. 24, no. 1, pp. 105–120, Mar. 2013.

[12] X. Cai, X. Li, R. Yuan, and Y. Hei, "Identification and mitigation of NLOS based on channel state information for indoor WiFi localization," in *Proc. Int. Conf. Wireless Commun. Signal Process. (WCSP)*, Oct. 2015, pp. 1–5.

[13] J. Xiao, K. Wu, Y. Yi, and L. M. Ni, "FIFS: Fine-grained indoor fingerprinting system," in *Proc. 21st Int. Conf. Comput. Commun. Netw. (ICCCN)*, Jul. 2012, pp. 1–7.

[14] S. M. Bokhari, S. Sohaib, A. R. Khan, M. Shafi, and A. U. R. Khan, "DGRU based human activity recognition using channel state information," *Measurement*, vol. 167, Jan. 2021, Art. no. 108245.

[15] Y. Ma, G. Zhou, and S. Wang, "WiFi sensing with channel state information: A survey," *ACM Comput. Surv.*, vol. 52, no. 3, pp. 1–36, Jul. 2019.

[16] N. Damodaran, E. Haruni, M. Kokhkharova, and J. Schäfer, "Device free human activity and fall recognition using WiFi channel state information (CSI)," *CCF Trans. Pervasive Comput. Interact.*, vol. 2, no. 1, pp. 1–17, 2020.

[17] A. Jalal, M. Mahmood, and A. S. Hasan, "Multi-features descriptors for human activity tracking and recognition in indoor-outdoor environments," in *Proc. 16th Int. Bhurban Conf. Appl. Sci. Technol. (IBCAST)*, Jan. 2019, pp. 371–376.

[18] S. Win and T. L. L. Thein, "Real-time human motion detection, tracking and activity recognition with skeletal model," in *Proc. IEEE Conf. Comput. Appl. (ICCA)*, Feb. 2020, pp. 1–5.

[19] H. Ma and H. Liu, "Research on human motion recognition system based on MEMS sensor network," in *Proc. IEEE 4th Adv. Inf. Technol., Electron. Autom. Control Conf. (IAEAC)*, Dec. 2019, pp. 2530–2534.

[20] Z. Chen and F. Cao, "The construction and approximation of a class of neural networks operators with ramp functions," *J. Comput. Anal. Appl.*, vol. 14, no. 1, pp. 101–112, 2012.

[21] R. Martinek, L. Danys, and R. Jaros, "Adaptive software defined equalization techniques for indoor visible light communication," *Sensors*, vol. 20, no. 6, p. 1618, Mar. 2020.

[22] L. Ying, X. Liu, M. Li, L. Sun, P. Xiu, and J. Yang, "How does intelligent manufacturing affects enterprise innovation? The mediating role of organisational learning," *Enterprise Inf. Syst.*, vol. 16, no. 4, pp. 1–38, 2021.

[23] X. Liu, Y. Li, Y. Li, S. Yu, and C. Tian, "The study on human action recognition with depth video for intelligent monitoring," in *Proc. Chin. Control Decis. Conf. (CCDC)*, Jun. 2019, pp. 5702–5706.

[24] Y. Zhang, Z. Zhang, Y. Zhang, J. Bao, Y. Zhang, and H. Deng, "Human activity recognition based on motion sensor using U-Net," *IEEE Access*, vol. 7, pp. 75213–75226, 2019.

[25] H. Nematallah, S. Rajan, and A.-M. Cretu, "Logistic model tree for human activity recognition using smartphone-based inertial sensors," in *Proc. IEEE SENSORS*, Oct. 2019, pp. 1–4.

[26] P. Meier, K. Rohrmann, M. Sandner, and M. Prochaska, "Application of magnetic field sensors for hand gesture recognition with neural networks," in *Proc. IEEE 1st Global Conf. Life Sci. Technol. (LifeTech)*, Mar. 2019, pp. 200–203.

[27] Z. Gu, J. Wang, F. Shen, K. Xu, D. Ye, J. Huangfu, C. Li, and L. Ran, "Blind separation of Doppler human gesture signals based on continuous-wave radar sensors," *IEEE Trans. Instrum. Meas.*, vol. 68, no. 7, pp. 2659–2661, Jul. 2019.

[28] Z. Liu and Z. Pan, "Near-field source localisation using a velocity sensor array," *IET Radar, Sonar Navigat.*, vol. 7, no. 7, pp. 727–735, Aug. 2013.

[29] H. Li, X. He, X. Chen, Y. Fang, and Q. Fang, "Wi-motion: A robust human activity recognition using WiFi signals," *IEEE Access*, vol. 7, pp. 153287–153299, 2019.

[30] H. Yan, Y. Zhang, Y. Wang, and K. Xu, "WiAct: A passive WiFi-based human activity recognition system," *IEEE Sensors J.*, vol. 20, no. 1, pp. 296–305, Jan. 2020.

[31] L. Guo, X. Wen, Z. Lu, X. Shen, and Z. Han, "WiRoI: Spatial region of interest human sensing with commodity WiFi," in *Proc. IEEE Wireless Commun. Netw. Conf. (WCNC)*, Apr. 2019, pp. 1–6.

[32] Y. Bai, Z. Wang, K. Zheng, X. Wang, and J. Wang, "WiDrive: Adaptive WiFi-based recognition of driver activity for real-time and safe takeover," in *Proc. IEEE 39th Int. Conf. Distrib. Comput. Syst. (ICDCS)*, Jul. 2019, pp. 901–911.

[33] S. Lolla and A. Zhao, "WiFi motion detection: A study into efficacy and classification," in *Proc. IEEE Integr. STEM Educ. Conf. (ISEC)*, Mar. 2019, pp. 375–378.

[34] L. Zhang, Q. Gao, X. Ma, J. Wang, T. Yang, and H. Wang, "DeFi: Robust training-free device-free wireless localization with WiFi," *IEEE Trans. Veh. Technol.*, vol. 67, no. 9, pp. 8822–8831, Sep. 2018.

[35] S. D. Domenico, M. D. Sanctis, E. Cianca, F. Giuliano, and G. Bianchi, "Exploring training options for RF sensing using CSI," *IEEE Commun. Mag.*, vol. 56, no. 5, pp. 116–123, May 2018.

[36] J. Liu, J. Yu, M. Li, L. Li, D. Li, and S. Shen, "Evolutionary game-based cooperative strategy for effective capacity of multiple-input-multiple-output communications," *Int. J. Distrib. Sensor Netw.*, vol. 13, no. 10, 2017, Art. no. 1550147717737969.

[37] Y. Song, T. Jin, Y. Dai, Y. Song, and X. Zhou, "Through-wall human pose reconstruction via UWB MIMO radar and 3D CNN," *Remote Sens.*, vol. 13, no. 2, p. 241, Jan. 2021.

[38] Y. Liu, "Human motion image detection and tracking method based on Gaussian mixture model and CAMSHIFT," *Microprocessors Microsystems*, vol. 82, Apr. 2021, Art. no. 103843.

[39] Z. Burciu, T. Abramowicz-Gerigk, W. Przybyl, I. Plebankiewicz, and A. Januszko, "The impact of the improved search object detection on the SAR action success probability in maritime transport," *Sensors*, vol. 20, no. 14, p. 3962, Jul. 2020.

[40] R. Jia, "Design of a simulation platform for intelligent marine search and rescue based on wireless sensors," *Microprocessors Microsystems*, vol. 80, Feb. 2021, Art. no. 103572.

[41] K. Naus, M. Wąż, P. Szymak, L. Gucma, and M. Gucma, "Assessment of ship position estimation accuracy based on radar navigation mark echoes identified in an electronic navigational chart," *Measurement*, vol. 169, Feb. 2021, Art. no. 108630.

[42] J. Maitre, K. Bouchard, C. Bertuglia, and S. Gaboury, "Recognizing activities of daily living from UWB radars and deep learning," *Expert Syst. Appl.*, vol. 164, Feb. 2021, Art. no. 113994.

[43] E. Miller, N. Banerjee, and T. Zhu, "Smart Homes that detect sneeze, cough, and face touching," *Smart Health*, vol. 19, Mar. 2021, Art. no. 100170.

[44] H. Li, X. He, X. Chen, Y. Fang, and Q. Fang, "Wi-motion: A robust human activity recognition using WiFi signals," *IEEE Access*, vol. 7, pp. 153287–153299, 2019.

[45] S. H. Javadi and A. Farina, "Radar networks: A review of features and challenges," *Inf. Fusion*, vol. 61, pp. 48–55, Sep. 2020.

[46] L. Chen, "Road vehicle recognition algorithm in safety assistant driving based on artificial intelligence," *Soft Comput.*, pp. 1–10, Jul. 2021.

[47] C. Ding, H. Hong, Y. Zou, H. Chu, X. Zhu, F. Fioranelli, J. Le Kernec, and C. Li, "Continuous human motion recognition with a dynamic range-Doppler trajectory method based on FMCW radar," *IEEE Trans. Geosci. Remote Sens.*, vol. 57, no. 9, pp. 6821–6831, Sep. 2019.

[48] Q. Zhai, X. Han, Y. Han, J. Yi, S. Wang, and T. Liu, "A contactless on-bed radar system for human respiration monitoring," *IEEE Trans. Instrum. Meas.*, vol. 71, pp. 1–10, 2022.

[49] R. Arai and K. Murakami, "Hierarchical human motion recognition by using motion capture system," in *Proc. Int. Workshop Adv. Image Technol. (IWAIT)*, Jan. 2018, pp. 1–4.

[50] N. Golestani and M. Moghaddam, "Magnetic induction-based human activity recognition (MI-HAR)," in *Proc. IEEE Int. Symp. Antennas Propag. USNC-URSI Radio Sci. Meeting*, Jul. 2019, pp. 17–18.

[51] S. Skaria, A. Al-Hourani, M. Lech, and R. J. Evans, "Hand-gesture recognition using two-antenna Doppler radar with deep convolutional neural networks," *IEEE Sensors J.*, vol. 19, no. 8, pp. 3041–3048, Apr. 2019.

[52] Z. Zhang, Z. Tian, and M. Zhou, "Latern: Dynamic continuous hand gesture recognition using FMCW radar sensor," *IEEE Sensors J.*, vol. 18, no. 8, pp. 3278–3289, Feb. 2018.

[53] C. Li, V. M. Lubecke, O. Boric-Lubecke, and J. Lin, "A review on recent advances in Doppler radar sensors for noncontact healthcare monitoring," *IEEE Trans. Microw. Theory Techn.*, vol. 61, no. 5, pp. 2046–2060, May 2013.

[54] T. A. Zilani, F. Al-Turjman, M. B. Khan, N. Zhao, and X. Yang, "Monitoring movements of ataxia patient by using UWB technology," *Sensors*, vol. 20, no. 3, pp. 1–16, 2020.

[55] X. Dai, Z. Zhou, J. J. Zhang, and B. Davidson, "Ultra-wideband radar based human body landmark detection and tracking with biomedical constraints for human motion measuring," in *Proc. 48th Asilomar Conf. Signals, Syst. Comput.*, Nov. 2014, pp. 1752–1756.

[56] X. Yang, W. Yin, and L. Zhang, "People counting based on CNN using IR-UWB radar," in *Proc. IEEE/CIC Int. Conf. Commun. China (ICCC)*, Oct. 2017, pp. 1–5.

[57] P. Cao, W. Xia, M. Ye, J. Zhang, and J. Zhou, "Radar-ID: Human identification based on radar micro-Doppler signatures using deep convolutional neural networks," *IET Radar Sonar Navigat.*, vol. 12, no. 7, pp. 729–734, Apr. 2018.

[58] P. Kalarani and S. S. Brunda, "An efficient approach for ensemble of SVM and ANN for sentiment classification," in *Proc. IEEE Int. Conf. Adv. Comput. Appl. (ICACA)*, Oct. 2016, pp. 99–103.

[59] F. Ahmad and M. G. Amin, "Noncoherent approach to through-the-wall radar localization," *IEEE Trans. Aerosp. Electron. Syst.*, vol. 42, no. 4, pp. 1405–1419, Oct. 2006.

[60] C. Debes, M. G. Amin, and A. M. Zoubir, "Target detection in single- and multiple-view through-the-wall radar imaging," *IEEE Trans. Geosci. Remote Sens.*, vol. 47, no. 5, pp. 1349–1361, May 2009.

[61] F. H. C. Tivive and A. Bouzerdoum, "Through-the-wall target separation using low-rank and variational mode decomposition," *IEEE Trans. Geosci. Remote Sens.*, vol. 57, no. 12, pp. 9928–9940, Dec. 2019.

[62] A. H. Muqaibel and A. A. Albeladi, "Dynamic joint reconstruction of walls and targets in through-the-wall radar imaging," *IEEE Access*, vol. 7, pp. 134028–134035, 2019.

[63] F. H. C. Tivive and A. Bouzerdoum, "Clutter removal in through-the-wall radar imaging using sparse autoencoder with low-rank projection," *IEEE Trans. Geosci. Remote Sens.*, vol. 59, no. 2, pp. 1118–1129, Feb. 2021.

[64] A. Rittiplang, P. Phasukkit, and T. Orankitanun, "Optimal central frequency for non-contact vital sign detection using monocycle UWB radar," *Sensors*, vol. 20, no. 10, p. 2916, May 2020.

[65] Y. Sun, S. Zhang, and Z. Cui, "Group sparsity based imaging algorithm for TWRI under wall parameter uncertainties," *Trans. Inst. Meas. Control*, vol. 40, no. 1, pp. 251–260, 2018.

[66] F. H. C. Tivive and A. Bouzerdoum, "Toward moving target detection in through-the-wall radar imaging," *IEEE Trans. Geosci. Remote Sens.*, vol. 59, no. 3, pp. 2028–2040, Mar. 2020.

[67] Y. Song, T. Jin, Y. Dai, Y. Song, and X. Zhou, "Through-wall human pose reconstruction via UWB MIMO radar and 3D CNN," *Remote Sens.*, vol. 13, no. 2, p. 241, Jan. 2021.

[68] F. H. C. Tivive and A. Bouzerdoum, "Clutter removal in through-the-wall radar imaging using sparse autoencoder with low-rank projection," *IEEE Trans. Geosci. Remote Sens.*, vol. 59, no. 2, pp. 1118–1129, Feb. 2021.

[69] S. Kianoush, S. Savazzi, V. Rampa, and M. Nicoli, "People counting by dense WiFi MIMO networks: Channel features and machine learning algorithms," *Sensors*, vol. 19, no. 16, p. 3450, Aug. 2019.

[70] A. Ghio, S. Escalante, and J. Tarrillo, "Analysis of moving average filter for IMU measurements on an 8-bit microcontroller," in *Proc. IEEE 25th Int. Conf. Electron., Electr. Eng. Comput. (INTERCON)*, Aug. 2018, pp. 1–4.

[71] W. S. Smith, "The scientist and engineer's guide to digital signal processing," California Technical Publishing, San Diego, CA, USA, Tech. Rep., 1997.

[72] S. Wang, Z. Chen, and B. Sheng, "Convergence rate of SVM for kernel-based robust regression," *Int. J. Wavelets, Multiresolution Inf. Process.*, vol. 17, no. 1, Jan. 2019, Art. no. 1950004.

[73] W. Buwei, C. Jianfeng, W. Bo, and F. Shuanglei, "A solar power prediction using support vector machines based on multi-source data fusion," in *Proc. Int. Conf. Power Syst. Technol. (POWERCON)*, Nov. 2018, pp. 4573–4577.

[74] I. Belakhdar, W. Kaaniche, R. Djmel, and B. Ouni, "A comparison between ANN and SVM classifier for drowsiness detection based on single EEG channel," in *Proc. 2nd Int. Conf. Adv. Technol. Signal Image Process. (ATSIP)*, Mar. 2016, pp. 443–446.

[75] Z. Yang, L. Kang, Y. Guo, H. Ma, and Z. Min, "Compact real-valued teaching-learning based optimization with the applications to neural network training," *Knowl.-Based Syst.*, vol. 159, pp. 51–62, Nov. 2018.

[76] E. Romero and D. Toppo, "Comparing support vector machines and feed-forward neural networks with similar hidden-layer weights," *IEEE Trans. Neural Netw.*, vol. 18, no. 3, pp. 959–963, May 2007.

[77] S. Ujan, N. Navidi, and R. J. Landry, "Hierarchical classification method for radio frequency interference recognition and characterization in satcom," *Appl. Sci.*, vol. 10, no. 13, p. 4608, Jul. 2020.

[78] A. J. Schoenwald, A. Gholian, D. C. Bradley, M. Wong, P. N. Mohammed, and J. R. Piepmeier, "RFI detection and mitigation using independent component analysis as a pre-processor," in *Proc. Radio Freq. Interference (RFI)*, Oct. 2016, pp. 100–104.

[79] O. Mosiane, N. Oozeer, and B. A. Bassett, "Radio frequency interference detection using machine learning," in *Proc. IEEE Radio Antenna Days Indian Ocean (RADIO)*, Oct. 2016, pp. 1–2.

[80] A. M. Llenas, J. Riihijarvi, and M. Petrova, "Performance evaluation of machine learning based signal classification using statistical and multiscale entropy features," in *Proc. IEEE Wireless Commun. Netw. Conf. (WCNC)*, Mar. 2017, pp. 1–6.

[81] M. Tarawneh and O. Embarak, "Hybrid approach for heart disease prediction using data mining techniques," in *Advances in Internet, Data and Web Technologies*, L. Barolli, F. Xhafa, Z. A. Khan, and H. Odhabi, Eds. Cham, Switzerland: Springer, 2019, pp. 447–454.

[82] A. P. Bradley, "The use of the area under the ROC curve in the evaluation of machine learning algorithms," *Pattern Recognit.*, vol. 30, no. 7, pp. 1145–1159, 1997.

[83] Z. Lei, Y. Sun, Y. A. Nanehkaran, S. Yang, M. S. Islam, H. Lei, and D. Zhang, "A novel data-driven robust framework based on machine learning and knowledge graph for disease classification," *Future Gener. Comput. Syst.*, vol. 102, pp. 534–548, Jan. 2020.

[84] (2022). *Mathworks*. Accessed: Mar. 15, 2022. [Online]. Available: https://www.mathworks.com/

[85] T. K. Kim, "T test as a parametric statistic," *Korean J. Anesthesiol*, vol. 68, no. 6, pp. 540–546, 2015.

[86] M. Hernandez, Y. Tchatchoua, T. Q. Nguyen, and D. Y. C. Lie, "A prototype novel zero-IF non-contact respiration monitor using software defined radio (SDR)," in *Proc. IEEE 63rd Int. Midwest Symp. Circuits Syst. (MWSCAS)*, Aug. 2020, pp. 69–72.

SAMEER AHMAD BHAT received the B.S. degree in information technology and the M.S. degree in computer science from the University of Kashmir, Jammu and Kashmir, India, in 2008 and 2011, respectively. He is currently pursuing the Ph.D. degree with the Gdańsk University of Technology, Gdańsk, Poland. From 2011 to 2016, he was with King Saud University, Saudi Arabia. From 2016 to 2021, he was with the Kuwait College of Science and Technology, Kuwait. From 2021 to 2022, he was with the Gulf University for Science and Technology, Kuwait. His research interests include AI and machine learning, sustainable development, e-heath, human motion activity and recognition systems, embedded systems and the Internet of Things, wireless power transfer, smart grid systems, educational technology, and human–computer interaction.

MUNEER AHMAD DAR received the M.S. degree in computer science from the University of Kashmir, Jammu and Kashmir, India, in 2004, the M.Phil. degree in computer science from Madurai Kamaraj University, India, in 2009, and the Ph.D. degree in computer science from the University of Kashmir, in 2019. He currently works as a Senior Researcher (Scientist-C) at the National Institute of Electronics and Information Technology, Srinagar (NIELIT Srinagar), Ministry of Electronics and Information Technology, Government of India. He also serves as the Head of Department of Computer Science and Information Technology, NIELIT. He is the author and coauthor of various conference papers and journal articles, and including various book chapters. His research interests include multiple areas of computer science and engineering. His current research interests include security of smartphone applications, network security, e-learning platforms, and AI and machine learning. He is an Active Member of the Institution of Electronics and Telecommunication Engineers (IETE) and the International Association of Engineers (IAENG) Group.

DALIA ALYAHYA received the M.A. degree in arts education from King Saud University (KSU), Saudi Arabia, in 2005, and the M.A. and Ph.D. degrees in educational technology from the University of Northern Colorado (UNC), Greeley, CO, USA, in 2011. She currently works as an Associate Professor with the Department of Instructional Technology, KSU. She is also an Advisor and a Consultant at the Heritage Commission, Ministry of Culture, Saudi Arabia. Her research interests include information visualization, eye tracking technology, instructional design and technology, and human–computer interaction.

PIOTR SZCZUKO received the D.Sc. degree in computer science from the Gdańsk University of Technology, Poland, in 2020. He is the author and coauthor of over 100 papers, book chapters, and articles. His research interests include processing of audio and video, computer animation, 3-D visualization, machine learning and artificial intelligence, applications of rough sets theory, classification, and perception of sound and image, and applications of embedded systems.

FARHANA MUSTAFA received the B.Tech. degree from Baba Gulam Shah Bad Shah University (BGBSU), in 2013, and the M.Tech. degree from the University of Pune, India, in 2015. She is currently pursuing the Ph.D. degree in electronics and communication engineering with the University of Kashmir, India. She is also working as an Assistant Professor. She has published research in various international journals and conference papers. Her research interests include wireless and communications, RF engineering, signal processing, MIMO systems, 5G communications, optimization methods, cellular networks, and artificial intelligence and machine learning.

∙ ∙ ∙